

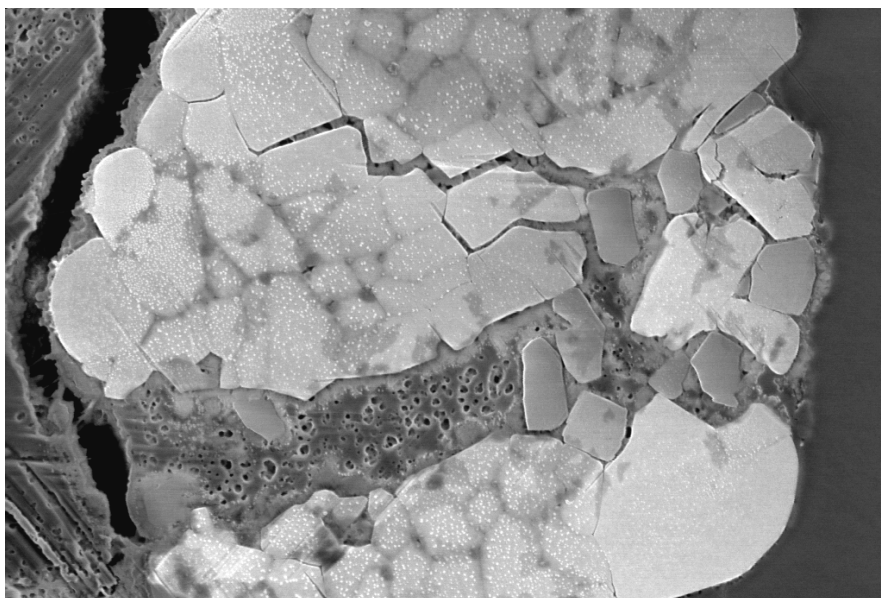


Doctoral Thesis in Fibre and Polymer Science

Hybrid polymer-liquid electrolytes for lithium ion battery applications

MARTINA CATTARUZZA

KTH ROYAL INSTITUTE OF TECHNOLOGY



Hybrid polymer-liquid electrolytes for lithium ion battery applications

MARTINA CATTARUZZA

Academic Dissertation which, with due permission of the KTH Royal Institute of Technology, is submitted for public defence for the Degree of Doctor of Philosophy on Friday the 25th October 2024, at 10:00 a.m. in E3, Osquars backe 18, floor 5, Stockholm

Doctoral Thesis in Fibre and Polymer Science
KTH Royal Institute of Technology
Stockholm, Sweden 2024

© Martina Cattaruzza

Cover page photo: Martina Cattaruzza

ISBN 978-91-8106-068-3
TRITA-CBH-FOU-2024:44

Printed by: Universitetservice US-AB, Sweden 2024

*To my mother,
my sister,
and all the other women who inspired me along the way.*

I. Abstract

The global shift towards renewable energy sources and the electrification of transportation necessitates advanced energy storage solutions, with lithium-ion batteries (LIBs) at the forefront. However, conventional batteries with liquid electrolytes in LIBs pose several limitations such as flammability, poor chemical stability, leakage risks, overall safety concerns, and limited processability. This thesis investigates hybrid polymer-liquid electrolytes (HEs) as an alternative to address these issues in LIBs as well as a way to obtain additional functionalities e.g. improved structural integrity.

The research is organized into four main studies. Paper I focuses on the three-dimensional (3D) reconstruction and analysis of HE structures. Using focused ion beam-scanning electron microscopy (FIB-SEM), the study reveals the complex, interconnected pore networks within HEs that are critical for ionic conductivity and mechanical stability.

Paper II explores the impact of porosity on the ionic and molecular mobility within HEs. By varying the liquid electrolyte content, the study demonstrates how increased porosity enhances ion mobility, directly correlating with improved electrochemical performance. Nuclear magnetic resonance (NMR) diffusion experiments further elucidate the transport mechanisms within the polymer matrix, showing a significant increase in ion diffusion rates with higher electrolyte content.

Paper III examines the role of nanosized carbon black (CB) particles in the polymerization-induced phase separation (PIPS) process used to synthesize HEs. The addition of CB improves the conductivity of HEs without compromising their morphological integrity. The study finds that even small

amounts of CB can substantially enhance the overall conductivity, making CB-rich HEs potential candidates for multifunctional roles within battery electrodes, such as conductive binders.

Paper IV evaluates the practical application of HEs by integrating them into commercial LIB electrodes. The HE-infused electrodes maintain their structural and electrochemical properties even after multiple charge-discharge cycles, proving their potential for use in commercial applications.

This thesis contributes to the development of multifunctional electrolytes that not only address the safety issues associated with liquid electrolytes but also advance multifunctionality in LIBs. The methodologies and findings presented provide a foundation for future research in high-performance, safer, and more sustainable battery technologies.

Keywords

Hybrid Polymer-Liquid Electrolytes, Lithium-Ion Batteries, Energy Storage

II. Sammanfattning

Den globala förändringen mot förnybara energikällor och elektrifieringen av transporter kräver avancerade energilagringssystem, med litiumjonbatterier (LIB) i framkant. Konventionella batterier med flytande elektrolyter i LIB har dock flera begränsningar såsom brandfarlighet, kemisk instabilitet, risk för läckage, begränsade bearbetbarhet och säkerhetsproblem. Denna avhandling undersöker ”hybrid polymer-liquid electrolytes” (HEs) som ett alternativ för att ta itu med dessa problem i LIBs samt ett sätt att erhålla ytterligare funktionaliteter t.ex. förbättrad strukturell integritet.

Forskningen är organiserad i fyra huvudstudier. Artikel I fokuserar på tredimensionell (3D) rekonstruktion och analys av HE-strukturer. Med hjälp av ”focused ion beam-scanning electron microscopy” (FIB-SEM) visar studien de komplexa, sammankopplade nätverken inom HEs som är avgörande för jonkonduktivitet och mekanisk stabilitet.

Artikel II utforskar inverkan av porositet på jonisk och molekylär rörlighet inom HEs. Genom att variera innehållet av flytande elektrolyt visar studien hur ökad porositet förbättrar jonmobiliteten, vilket direkt korrelerar med förbättrad elektrokemisk prestanda. ”Nuclear magnetic resonance” (NMR) diffusionsexperiment belyser transportmekanismerna inom polymermatrisen ytterligare och visar en signifikant ökning av jondiffusionshastigheter med högre elektrolythalt.

Artikel III undersöker rollen av kimrökspartiklar (CB) i nanostorlek i den polymerisationsinducerade fasset separationsprocessen (PIPS) som används för att syntetisera HE. Tillsatsen av CB förbättrar konduktiviteten hos HE utan att kompromissa med deras morfologiska integritet. Studien visar att även små

mängder CB avsevärt kan förbättra den totala konduktiviteten, vilket gör CB-rika HEs potentiella kandidater för multifunktionella roller inom batterielektroder, såsom ledande bindemedel.

Artikel IV utvärderar den praktiska tillämpningen av HE:er genom att integrera dem i kommersiella LIB-elektroder. De HE-innehållande elektroderna bibehåller sina strukturella och elektrokemiska egenskaper även efter flera laddnings-URLaddningscykler, vilket bevisar deras potential för användning i kommersiella tillämpningar.

Denna avhandling bidrar till utvecklingen av multifunktionella elektrolyter som inte bara tar upp säkerhetsfrågorna förknippade med flytande elektrolyter utan också främjar multifunktionaliteten i LIB. Metoderna och resultaten som presenteras ger en grund för framtida forskning inom högpresterande, säkrare och mer hållbar batteriteknologi.

Nyckelord

Hybrid polymer-vätske elektrolyter, Litiumjonbatterier, Energilagring

III. List of publications

- i. S. Duan, **M. Cattaruzza**, V. Tu, R. M. Auenhammer, R. Jänicke, M. K. G. Johansson, F. Liu, and L. E. Asp, "Three-dimensional reconstruction and computational analysis of a structural battery composite electrolyte", *Communications Materials*, vol. 4, no. 1, 2023.
- ii. **M. Cattaruzza**, Y. Fang, I. Furó, G. Lindbergh, F. Liu, and M. Johansson, "Hybrid polymer–liquid lithium ion electrolytes: effect of porosity on the ionic and molecular mobility", *Journal of Materials Chemistry A*, vol. 11, no. 13, pp. 7006-7015, 2023.
- iii. **M. Cattaruzza**, Y. Fang, I. Furó, G. Lindbergh, F. Liu, and M. Johansson, "Hybrid polymer–liquid lithium ion electrolytes: effect of carbon black during polymerization-induced phase separation", *ACS Applied Energy Materials*. *Revised manuscript submitted, August 2024.*
- iv. **M. Cattaruzza**, G. Lindbergh, M. Johansson, and F. Liu, "Hybrid polymer-liquid electrolytes and their interactions with electrode materials". *Manuscript submitted, September 2024.*

IV. Contributions to the appended publications

- I. Experimental design, sample manufacturing, electrochemical and mechanical characterization, data processing, result interpretation and discussion, and writing of the article.
- II. Experimental design, sample manufacturing, sample characterization, data processing, result interpretation and discussion, and writing of the article.
- III. Experimental design, sample manufacturing, sample characterization, data processing, result interpretation and discussion, and writing of the article.
- IV. Experimental design, sample manufacturing, sample characterization, data processing, result interpretation and discussion, and writing of the article.

V. List of publications not included in the thesis

- i. G. Maffei, S. Emilsson, **M. Cattaruzza**, and M. Johansson, "Effect of monomer composition on the formation of hybrid polymer-liquid electrolytes for lithium-ion batteries". *Manuscript under preparation*.
- ii. E. Lind, **M. Cattaruzza**, D. Zenkert, M. Johansson, and G. Lindbergh, "Electrochemical Solid Polymer Electrolyte Coating of Carbon Fibres for Structural Sodium Micro Batteries". *Manuscript under preparation*.
- iii. Å. Jerlhagen, K. Gordeyeva, **M. Cattaruzza**, L. Brandt, B. Sochor, S. K. Vayalil, S. V. Roth, L. Wågberg, and E. Malmström, "Decoding in-plane orientation of self-assembled structures in cellulose nanopapers hybridized with tailored polymeric nanoparticles". *Manuscript submitted, 2024*.
- iv. L. M. Schneider, **M. Cattaruzza**, S. Emilsson, Dan Zenkert, G. Lindbergh, and M. Johansson, "The Effect of Electrolyte Composition on Biphasic Structural Electrolytes for Laminated Structural Batteries". *Manuscript under preparation*.
- v. V. Matovic, **M. Cattaruzza**, and F. Liu, "Revealing the complex nano porous structure of a polymer hybrid electrolyte aided by deep learning". *Manuscript under preparation*.

VI. List of abbreviations

AIBN	2,2'-azobis(2-methylpropionitrile)
ATR	attenuated total reflection
BIB	broad ion beam
BMS	battery management system
BPAMA	bisphenol A ethoxylate dimethacrylate
CB	carbon black
DMA	dynamic mechanical analysis
EC	ethylene carbonate
EIS	electrochemical impedance spectroscopy
FEM	finite element method
FIB	focused ion beam
FTIR	Fourier-transform infrared spectroscopy
GHGs	greenhouse gases
GPEs	gel polymer electrolytes
HEs	hybrid polymer-liquid electrolytes
IPCC	Intergovernmental Panel on Climate Change

LFP	lithium iron phosphate
LIBs	lithium-ion batteries
LiTFSI	lithium bis(trifluoromethanesulfonyl)imide
NMC	lithium nickel manganese cobalt oxide
NMP	N-methylpyrrolidone
NMR	nuclear magnetic resonance
PC	propylene carbonate
PEO	polyethylene oxide
PFAS	per- and polyfluoroalkyl substances
PIPS	polymerization-induced phase separation
PVDF	polyvinylidene fluoride
SBEs	structural battery electrolytes
SBs	structural batteries
SDGs	sustainable development goals
SEM	scanning electron microscopy
SPEs	solid polymer electrolytes
UN	United Nations

CONTENTS

1	Introduction	1
1.1	Background	1
1.2	Lithium-ion batteries	3
1.3	Polymer electrolytes	6
1.4	Hybrid polymer-liquid electrolytes	7
1.5	Electrodes	8
1.6	Electrode additives	9
1.7	Multifunctionality of HEs.....	11
1.7.1	HEs as structural battery electrolytes	11
1.7.2	HEs as binders and separators	11
1.8	Purpose of the study	13
2	Materials & Methods	15
2.1	Materials	15
2.2	Sample preparation.....	16
2.2.1	HE and bulk polymer film manufacturing.....	16
2.2.2	HE-infused electrode and half-cell manufacturing.....	17
2.3	Characterization techniques	17
2.3.1	Microscopy characterization	17
2.3.2	Mechanical characterization	20
2.3.3	Spectroscopy characterization	20
2.3.4	Electrochemical characterization	22
3	Results & Discussion	25
3.1	Paper I: 3D reconstruction and modelling of HE, theoretical models vs experimental data	25
3.1.1	3D reconstruction of the HE	26
3.1.2	Geodesic tortuosity.....	27
3.1.3	Simulated data vs experimental data.....	29
3.2	Paper II: effect of porosity on the ionic and molecular mobility in HEs .	31
3.2.1	Curing performance.....	31
3.2.2	Ionic and molecular mobility.....	31
3.2.3	Morphology and structure	34
3.3	Paper III: effect of nanosized carbon black particles on HEs	35
3.3.1	Curing performance.....	35
3.3.2	Ionic and molecular mobility.....	36
3.3.3	Morphology and structure	38
3.4	Paper IV: HEs interactions with electrodes	40

3.4.1	Infusion and PIPS in electrodes.....	40
3.4.2	Interface formation and stability.....	41
3.4.3	Cycling performance.....	45
4	Conclusions.....	47
5	Future Work.....	49
6	Acknowledgments.....	53
7	References.....	57

1 Introduction

1.1 Background

Decades of increased consumption have led to significant global environmental changes, most notably rising global temperatures. The Intergovernmental Panel on Climate Change (IPCC) warned in 2014 that, without intervention, global average temperature could exceed 4 °C above pre-industrial levels by the end of this century [1]. Such an increase would have catastrophic effects, including increased droughts, more extreme weather events, irreversible biodiversity loss, mass extinctions, and rising sea levels, impacting billions of people worldwide [2]. Global warming is driven by the accumulation of greenhouse gases (GHGs) in the atmosphere, which trap solar radiation and disrupt long-established weather patterns, causing a net increase in global temperature [3]. There is a growing consensus that humanity must change its current trajectory to ensure lasting prosperity for future generations. In response, numerous international initiatives aim to address the issue. The Paris Agreement, signed by 191 countries in 2016, seeks to limit global warming to well below 2 °C, ideally capping it at 1.5 °C by the end of the 21st century [4]. This requires a dramatic reduction in GHGs emissions over the coming decades, necessitating both societal changes and technological innovations. As the energy sector relies heavily on burning fossil fuels, it is responsible for approximately 73% of global GHGs emissions, including those associated with energy use in industries, buildings, and transport [5]. To address the significant contribution of fossil fuels to GHG emissions, a critical focus must be placed on expanding renewable energy sources, which provide a sustainable alternative to reduce reliance on

carbon-intensive energy and pave the way for a cleaner future. However, the challenge with renewable energy sources is their intermittent nature, as solar and wind power generation depend on weather conditions and time of day. Therefore, the integration of renewable energy sources with efficient energy storage systems and the electrification of the transportation sector are a pivotal shift in addressing climate change, reducing greenhouse gas emissions, and achieving sustainable development goals (SDGs).

The United Nations (UN) established the SDGs as a universal call to action to end poverty, protect the planet, and ensure prosperity for all by 2030 [6]. Among the 17 goals, several are directly impacted by advancements in energy storage research, which is addressed in the present research. Goal 7, Affordable and Clean Energy, is significantly supported by the development of advanced energy storage technologies, which are essential for integrating renewable energy sources like solar and wind into the grid, thus promoting clean energy access. Goal 9, Industry, Innovation, and Infrastructure, is advanced through the enhancement of energy storage technologies, fostering sustainable industrial processes and innovative energy solutions. Goal 11, Sustainable Cities and Communities, benefits from the electrification of transportation, reducing urban air pollution and dependence on fossil fuels. Lastly, Goal 13, Climate Action, is addressed by reducing greenhouse gas emissions through the widespread adoption of renewable energy and electric vehicles, contributing to the transition towards a low-carbon economy.

1.2 Lithium-ion batteries

The advent of lithium-ion batteries (LIBs) in the 1970s has revolutionized the electrochemical energy storage field, causing LIBs to emerge as the leading rechargeable energy storage technology and transform various industry sectors such as portable electronics and electric vehicles [7, 8]. The significance of LIBs was recognized in 2019 when John B. Goodenough, M. Stanley Whittingham, and Akira Yoshino were awarded the Nobel Prize in Chemistry for their contributions to the development of this technology [9, 10].

Widespread adoption of LIBs is attributed to their high energy density, long cycle life, and relatively low self-discharge rate compared to traditional battery chemistries [11]. Lithium is selected for battery technologies due to its highly electropositive and lightweight nature (0.535 g/cm^3), fulfilling the essential requirements for efficient battery formation [12]. Figure 1 shows the LIB components along with its operational principles. LIBs operate by transforming chemical energy into electrical energy via redox reactions. The working principle of LIBs involves the movement of lithium ions between two electrodes having different electrochemical potentials, the negative electrode (anode) and the positive electrode (cathode), which are immersed in an ionically conductive material called the electrolyte [13]. Electrolytes comprise lithium salts dissolved in organic solvents [14]. A separator, which is a porous polymer membrane, is situated between the electrodes to prevent electrical short circuits while allowing lithium ions to pass through [15]. Current collectors are commonly made of copper (for the anode) and aluminum (for the cathode) and allow the flow of electrons to and from the external circuit [16]. The operation of a LIB relies on the reversible transfer of lithium ions during charging and discharging cycles. This process involves electrochemical redox reactions at the surfaces of the electrodes and the intercalation of lithium ions within the electrodes. During charging, an external current is applied, causing lithium ions to move from the cathode to the anode through the electrolyte (cathode oxidation, anode reduction). Concurrently, electrons travel through the external circuit from the cathode to the anode, ensuring charge balance. Once the lithium ions reach the anode surface they intercalate into the structure of the negative electrode. During discharging, the battery supplies electrical energy to an external load as lithium ions spontaneously deintercalate from the anode and travel back to the cathode (anode oxidation, cathode reduction) through the electrolyte, while electrons flow through the external circuit from the anode to the cathode.

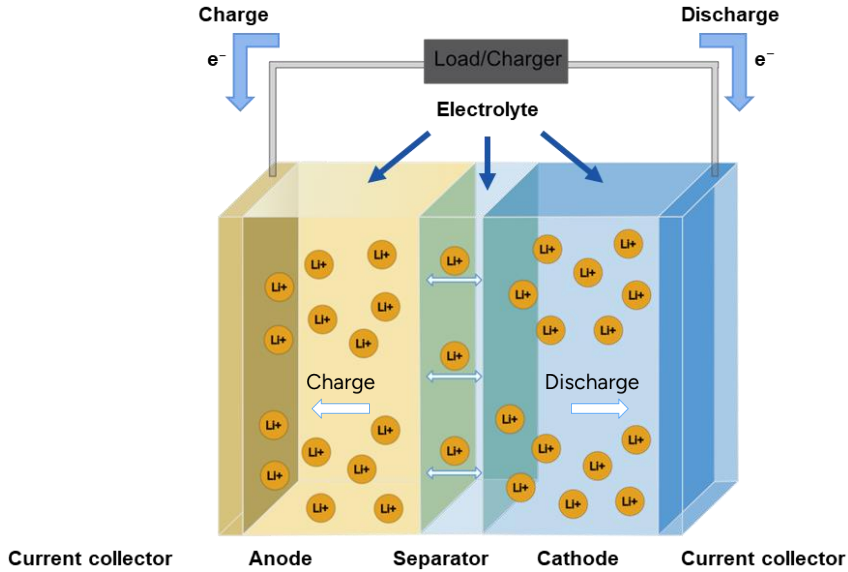
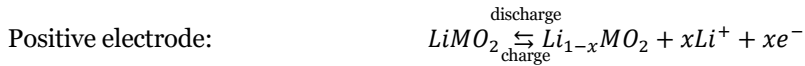


Figure 1: Illustration of a lithium-ion battery cell.

The electrochemical electrode reactions are as follows:



Where M represents a transition metal such as cobalt or manganese while C₆ represents graphite.

There are several key parameters when it comes to the LIBs characterization and performance [17]. Energy density refers to the amount of energy a battery can store relative to its weight or volume. It is typically expressed in watt-hours per kilogram (Wh/kg) or watt-hours per liter (Wh/L). High energy density allows for longer runtimes without increasing the battery size or weight. Power density refers to the amount of power (rate of energy delivery) a battery can provide

relative to its weight or volume. It is typically expressed in watts per kilogram (W/kg) or watts per liter (W/L). Power density indicates how quickly a battery can deliver energy to a device or system. The capacity of a battery, typically measured in ampere-hours (Ah), represents the total amount of electric charge it can store. Higher capacity batteries can power devices for longer periods without needing a recharge. The charging and discharging rate, often referred to as the C-rate, defines how quickly a battery can be charged or discharged. A higher C-rate allows for faster charging and discharging, but it must be managed carefully to avoid capacity loss, thermal issues and safety concerns. The weight of the battery is particularly important in applications such as electric vehicles, where a lighter battery contributes to better efficiency, longer range, and easier handling. Coulombic efficiency, a measure of how much charge is retained after each charge-discharge cycle, is critical for assessing the battery's long-term performance and capacity retention. Cycle life is the number of complete charge and discharge cycles a battery can undergo before its capacity falls below a specified percentage of its original capacity (often 80%). Chemical stability refers to the ability of the battery materials to resist degradation over time, which is crucial for maintaining performance and safety under various operating conditions. Voltage windows define the operational voltage range of the battery, within which it can safely and efficiently operate.

The manufacturing process of LIBs involves precise control over the assembly of battery components, such as the layering of electrodes, the quality control of electrolyte filling, and the assembly of cells into battery packs. These manufacturing aspects are crucial not only for achieving high initial performance but also for ensuring the consistency, reliability, and safety of the batteries throughout their operational life [18]. Finally, safety is a paramount concern in LIB design, as these batteries must be engineered to prevent hazardous conditions such as thermal runaway, which can lead to fires or explosions [19].

A battery system is composed of different levels of assembly, starting with the battery cells, which are the fundamental electrochemical units that store and release energy. These cells are combined to form battery modules, where multiple cells are connected in series and/or parallel to increase the overall voltage and capacity. The modules are then integrated into a larger assembly called a battery unit or battery pack, which includes several modules connected together to meet the specific energy and power demands of an application. This battery pack typically incorporates additional components like a battery

management system (BMS), thermal management systems, and safety mechanisms, ensuring that the entire system operates efficiently and safely in devices such as electric vehicles, drones, or portable electronics [20, 21].

1.3 Polymer electrolytes

Traditional liquid electrolytes used in LIBs present several significant limitations, including leakage, flammability, and thermal instability [14, 22]. These issues pose substantial safety risks, particularly in high-energy-density applications such as electric vehicles and portable electronics. Polymer electrolytes offer improved safety and performance due to their solid or semi-solid nature, which reduces the risk of leakage and enhances thermal stability. The concept of polymer electrolytes dates back to the 1970s when it was discovered that polyethylene oxide (PEO) could dissolve alkali metal salts, leading to ionic conductivity in a solid polymer matrix [23, 24].

This pioneering work laid the foundation for the development of solid polymer electrolytes (SPEs) [24, 25]. SPEs are composed of a polymer matrix such as PEO that is capable of dissolving and transporting ionic species, enabling ionic conduction through the movement of polymer chains. SPEs offer significant advantages over liquid electrolytes, including enhanced safety due to their non-flammable nature, superior mechanical strength, and greater thermal stability, reducing the risk of leakage and combustion at high temperatures. However, they often suffer from high electrode-electrolyte interfacial resistance and lower ionic conductivity at room temperature ranging between 10^{-8} - 10^{-5} S/cm compared to $>10^{-3}$ S/cm for liquid electrolytes, which can limit the battery's performance.

One solution to improve the polymer electrolytes ionic conductivity is gel polymer electrolytes (GPEs), which represent an intermediate state between liquid electrolytes and SPEs, consisting of a liquid phase evenly distributed throughout the polymer, forming a gel-like structure where the polymer matrix is swollen by the liquid electrolyte [26]. In the case of GPEs, the polymer backbone doesn't need to conduct ions as it is mainly the swelling liquid phase that is responsible for ionic conduction, with a range of 10^{-4} - 10^{-3} S/cm. GPEs are also mechanically flexible, making them suitable for flexible and wearable electronic applications, and they offer improved safety compared to liquid electrolytes due to reduced leakage risk and lower flammability [27]. While GPEs are flexible, their mechanical strength can sometimes be an issue which can lead to battery performance degradation over time [28].

1.4 Hybrid polymer-liquid electrolytes

Another promising example of polymer electrolytes is the hybrid polymer-liquid electrolytes (HEs) which involves the creation of a phase-separated system, where the polymer and liquid components exist as distinct phases within the electrolyte. HEs exhibit higher ionic conductivity (10^{-5} - 10^{-4} S/cm)[29] than SPEs due to the presence of the liquid component, which enables ion transport. In these systems the polymer is often cross-linked to establish a three-dimensional molecular structure that encapsulates the liquid component consisting of conventional lithium salts and organic solvents similar to those used in traditional LIBs. Thanks to the incorporation of the liquid phase within the polymer phase, HEs mitigate problems associated with volatility and leakages of liquid electrolytes without sacrificing the mechanical strength like in GPEs systems, thereby enhancing safety and structural integrity at the same time. HEs can be synthesized using a process known as polymerization-induced phase separation (PIPS), [30-34] wherein the phase separation occurs concurrently with the polymerization process due to the different solubilities of the monomers and the resulting polymer in the liquid electrolyte phase. The use of PIPS was pioneered as a method for creating heterogeneous electrolytes through stepwise polymerizing systems in conjunction with ionic liquids [35-38]. Later, PIPS was also implemented with free radical polymerization methods [29] where the polymerization proceeds by chain-wise propagation [39]. A common method for initiating the reaction is by using thermally or UV-light activated initiators, which are extensively used in making thermosets. Initially, a homogeneous mixture of monomer, solvents, lithium salt, and initiator is prepared, ensuring complete dissolution due to their similar solubility parameters. As polymerization begins, the monomers react, forming polymer chains and altering the mixture's solubility parameters, causing the newly formed polymer to become less soluble in the mixture. This leads to the separation of the mixture into two distinct phases: a polymer-rich phase and a percolating liquid solvent-rich phase, resulting in a bi-continuous network structure. A schematic of the PIPS reaction mechanism is represented in Figure 2.

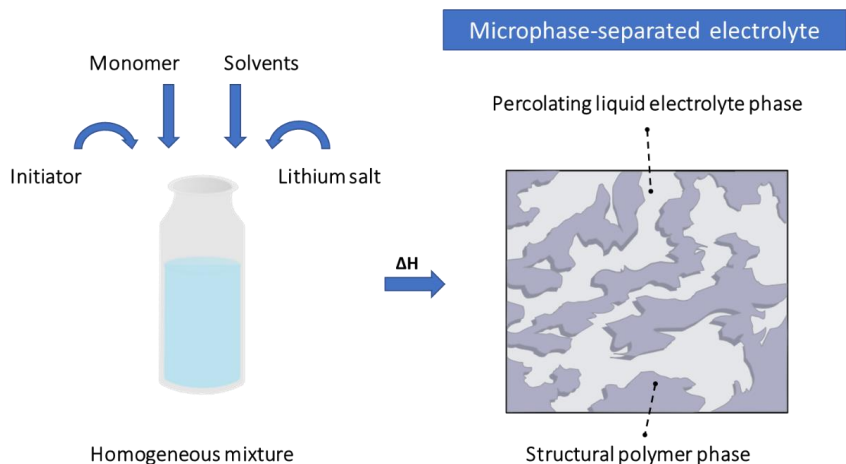


Figure 2: Schematic representation of the PIPS mechanism.

The polymer-rich phase forms a porous solid, interconnected network providing mechanical strength and dimensional stability to the HE, while the solvent-rich phase, trapped within the pores of this network, acts as a mobile phase for lithium ions transportation. A significant advantage when synthesizing HEs via PIPS is that, considering the low viscosity of the homogeneous HE precursor mixtures, the resins can be infused on any substrate and subsequently cured in-situ, allowing for precise control over the polymerization process in a one-step reaction [30]. Several factors influence the PIPS process, including monomer type and concentration, lithium salt type and concentration, polymerization temperature, and the solvents used [31, 40].

1.5 Electrodes

Another key component in a battery is the electrodes. Commercial LIB electrodes are predominantly intercalating materials, which means they store charge by incorporating lithium ions into their crystal structure. The most widely used anodic material in commercially available LIBs is graphite due to its high specific capacity of 372 mAh/g and its favorable electrochemical and mechanical stability [41-43]. Unlike the anode, there is not a single predominant cathode material. A variety of lithium transition-metal oxides are commonly used [44], consisting of layered olivine or spinel structures [45].

Lithium nickel manganese cobalt oxide's (NMC) layered structure enables high theoretical specific capacity (150-200 mAh/g depending on the nickel content), high nominal voltage (3.7–3.8 V) and excellent charge/discharge efficiency,

which are crucial for applications such as electric vehicles and portable electronics. The material's composition can be tailored to optimize specific properties: increasing nickel content enhances energy density, while higher manganese and cobalt contents improve stability and longevity [46]. This versatility allows manufacturers to customize NMC formulations to meet varying requirements for different applications.

Lithium iron phosphate (LFP) has gained widespread use in LIBs due to its exceptional safety, long cycle life, and thermal stability. Unlike other cathodes, LFP's olivine structure provides robust stability and resists overheating and thermal runaway, making it safer for high-demand applications. Additionally, LFP batteries exhibit excellent cycle life, maintaining capacity over thousands of charge-discharge cycles. While LFP has a lower theoretical specific capacity (170 mAh/g) and lower nominal voltage (3.2–3.3 V) compared to NMC, its environmental friendliness, cost-effectiveness, and safety make it ideal for applications where durability and safety are paramount [47].

The traditional manufacturing process for LIB electrodes involves mixing the electrode components—active material, binder, and conductive additive—with a solvent or solvent mixture to create a homogeneous slurry. This slurry is then applied to metal foils (aluminum for the cathode and copper for the anode), dried, and compacted to the desired thickness (this process is called calendaring). The electrodes are subsequently slit and wound before being assembled with separators and counter electrodes to form a battery cell, which is then infused with liquid electrolyte [48].

1.6 Electrode additives

Additives like electrically conductive materials and polymeric binders are incorporated into the LIB electrodes formulations to enhance their performance.

Electrically conductive materials, such as carbon black (CB), are integrated into the electrode formulations to improve electrical conductivity. These materials create an electrically conductive network within the electrode, facilitating the efficient movement of electrons and thereby enhancing the charge-discharge rates of the battery. The inclusion of these conductive additives is particularly important for the cathode, which generally has lower electronic conductivity compared to the anode. Although active materials present in anodes exhibit higher electronic conductivity than the ones present in cathodes, they tend to expand during charge-discharge cycles. This expansion can lead to the

degradation of anodes over time, resulting in the formation of inactive 'dead' materials that significantly reduce the anode's capacity after multiple cycles. CB in anode electrodes is already used to maintain good electronic conductance and to mitigate the issue of material delamination. By improving/maintaining the electrode's conductivity, CB helps to achieve faster kinetics and higher power density in LIBs. Moreover, the porous nature of CB is crucial for absorbing and retaining electrolyte, ensuring close contact between lithium ions and the electrodes' active materials [49]. Therefore, electrolyte compatibility with CB particles is essential for optimal LIB performance. A suitable electrolyte should effectively wet the CB surface, facilitating efficient ion transport during charge and discharge, leading to higher reliability and longevity of LIBs [50]. There are various types of CB, most of which are nanosized, highly porous, and electrically conductive [51]. In LIBs, a typical CB has a particle size ranging from 10 to 100 nm and a surface area of approximately 50 to 200 m²/g [52, 53].

Binders are essential components in both the cathode and anode, where they serve to hold the active material particles together and secure them to the current collectors. Binders help to create a cohesive and conductive network in conjunction with conductive additives like CB. Additionally, they manage the mechanical stresses associated with the expansion and contraction of anodes, preventing cracking and delamination. Different binders are used for anodes and cathodes in lithium-ion batteries due to the distinct chemical requirements of these electrodes and they can be categorized based on their solvent type into oil-soluble and water-soluble binders. One of the earliest and still widely used oil-soluble binders for LIB cathodes is polyvinylidene fluoride (PVDF) as it can withstand the cathodic oxidative environment. Despite using N-methylpyrrolidone (NMP) as a solvent, which is harmful to the environment, PVDF remains popular due to its high mechanical strength, good wear resistance, and excellent chemical stability. As a result, PVDF continues to dominate the market for cathode binders [54].

The European Commission is proposing a ban on all per- and polyfluoroalkyl substances (PFAS) due to their persistence, toxicity, and potential to bioaccumulate in organisms, including humans [55]. This includes all fluoropolymers like PVDF, a major subset of PFAS. Given this proposed ban, it is crucial to find alternatives to PVDF to comply with upcoming regulations and to reduce the environmental and health risks associated with PFAS.

1.7 Multifunctionality of HEs

Other than overcoming some of the problems associated with liquid electrolytes/SPEs/GPEs, HEs are emerging as multifunctional energy materials, with significant potential to revolutionize battery technology. They integrate the mechanical stability of solid polymers with the high ionic conductivity of liquid electrolytes, positioning themselves as key players in the development of next-generation energy storage systems. This dual capability makes them highly suitable for use in structural batteries (SBs) and other multifunctional energy storage applications, where they can potentially serve both as binders and separators within a cell setup.

1.7.1 HEs as structural battery electrolytes

Traditional battery components are designed solely for energy storage. The concept of SBs originated from the idea of integrating energy storage directly into the structural materials, thereby allowing for multifunctional components that can provide both mechanical support and electrical energy, inspired by the growing need for lightweight and efficient energy storage solutions in aerospace and automotive industries [56, 57]. Early studies on vinyl ester resins and epoxy resins [31, 33, 58-61] paved the way for the development of multifunctional structural battery electrolytes (SBEs) for SBs applications [29, 53, 62-69]. In the SBs, carbon fibers are used for both mechanical reinforcement and as electrodes due to their mechanical strength, ability to intercalate lithium ions and electrical conductivity [70-74]. SBEs are essentially HEs specifically designed for use in SBs, combining mechanical integrity with ionic conductivity to enable multifunctional energy storage. The polymer matrix within HEs provides mechanical support and load transfer to carbon fibers reinforcement, while the liquid component ensures efficient ion transport, enabling the electrolyte to maintain high performance under physical stress.

1.7.2 HEs as binders and separators

Beyond their role in SBs, HEs offer a versatile and innovative solution in battery manufacturing, potentially serving as binders and separators.

A binder should possess strong adhesion properties to securely bind electrode components while maintaining structural integrity throughout charge and discharge cycles. It should also have a good electrochemical stability, facilitate ionic conduction, and exhibit compatibility with the electrolyte, thereby enhancing the electrode-electrolyte interface and ultimately leading to higher

battery efficiency and longevity [75]. Since the HE fulfills all the aforementioned characteristics, it represents a suitable candidate which can be synthesized in a single-pot process replacing traditional fluorine-rich binders like PVDF where the use of harmful organic solvents is required. This not only reduces environmental impact but also simplifies the manufacturing process, potentially lowering production costs and improving sustainability.

Another potential application of HEs is their use as separators in batteries. The separator is a crucial component that prevents physical contact between the anode and cathode while allowing ionic transport. Separators, which are electrochemically inactive components, determine ionic transport between the electrodes as well as mechanical and thermal stability of the cell. A good battery separator must meet several requirements, including strong mechanical properties, high ionic conductivity, good wettability with electrolytes, and a uniform pore structure. Conventional separators, typically made from porous polyolefin membranes, are often the weak link in terms of thermal stability and safety [15]. Separators synthesized via PIPS have been previously tested using a single-step manufacturing technique [76, 77]. In a similar way, HE can serve as both an electrolyte and a separator, simplifying the battery design and manufacturing process. Their inherent ionic conductivity allows for efficient ion transport, while their polymer matrix provides the necessary mechanical strength and thermal stability. This dual function not only enhances battery safety by reducing the risk of short circuits and thermal runaway but also streamlines the manufacturing process, offering a pathway to more environmentally friendly and cost-effective battery production.

1.8 Purpose of the study

The scope of this thesis includes the development of a comprehensive workflow to reconstruct and analyze the structure and properties of HEs. The research presented in this thesis seeks to address several key questions aimed at deepening our understanding of HEs and their application in LIBs.

In Paper I, we investigate the three-dimensional morphology and tortuosity mapping of HEs, aiming to elucidate the structural characteristics that influence ionic conductivity and mechanical properties. High-resolution images of HEs were captured using focused ion beam (FIB) - scanning electron microscopy (SEM). The information was used to create detailed 3D models of the polymer and pore phases. These models enabled the analysis of pore size distribution and tortuosity, while the elastic modulus and ionic conductivity were both experimentally measured and numerically simulated for comparison and discussion.

In Paper II, we explore how the morphology and chemical composition of HEs impact molecular transport within the system, particularly focusing on how these factors affect ion mobility and overall electrochemical performance. HEs with different liquid content percentages were synthesized via PIPS. The ion conduction mechanisms were studied through morphological and nuclear magnetic resonance (NMR) studies, to give insights into the distribution and mobility of electrolytes within the two-phase HEs. The study moreover reveals the importance of the interplay between the two phases.

In paper III, the study examines the role of nanosized CB particles in the PIPS process, assessing its compatibility with HE constituents and its influence on the resulting structures and properties of HEs. HEs with different CB content percentages were synthesized via PIPS and their polymerization kinetics, morphology, and ionic and molecular mobility were evaluated at varying CB contents. This study shows the potential of using CB-rich HEs as conductive binders in electrode manufacturing through a one-pot process.

Finally, in Paper IV, we evaluate the feasibility of manufacturing battery half-cells using our developed HEs in commercial electrodes. This includes assessing whether the morphology and functionality of the HE-integrated system was possible to achieve with nano-sized and micron-sized active material particles in commercial electrodes and if the system remains stable during electrochemical cycling, accommodating the dimensional changes associated with charge and discharge cycles.

2 Materials & Methods

An overview of the materials and performed experimental techniques utilized is given below. Full data can be found in the appended papers.

2.1 Materials

The monomer bisphenol A ethoxylate dimethacrylate (BPAMA) (Mn: 540 g/mol) was provided by Sartomer (Arkema Group). Ethylene carbonate (EC), propylene carbonate (PC), lithium bis(trifluoromethanesulfonyl)imide (LiTFSI) (99.95% trace metal basis), lithium standard (used in paper II) 1000 mg/L in nitric acid (TraceCERT®) and thermal initiator 2,2'-azobis(2-methylpropionitrile) (AIBN) were purchased from Sigma-Aldrich. The commercial liquid electrolyte (used in paper III and paper IV) 1 M lithium bis(trifluoromethanesulfonyl)imide (LiTFSI) in a 1:1 v/v mixture of ethylene carbonate (EC) and propylene carbonate (PC), with 99.9% purity, was purchased from Solvionic. Carbon black (Super-P, TIMCAL) with a particle size of approximately 40 nm, a BET surface area of 57.0 – 67.0 m²/g, and a density of 160 ± 20 kg/m³ was purchased from Alfa Aesar (Thermo Scientific Chemicals). Lithium iron phosphate (LiFePO₄) with 90% active material content, a specific capacity of 150 mAh/g, a nominal voltage of 3.4 V vs Li/Li⁺, an area capacity of 2 mAh/cm² (±0.1 mAh/cm²), a density of 1.6 g/cm³ (±0.1 g/cm³), and a porosity of 57% (±4%) was purchased from Customcells Holding GmbH and was single-side coated on 20 μm thick aluminum current collector foils. Lithium nickel manganese cobalt oxide (LiNi_{0.8}Mn_{0.1}Co_{0.1}O₂, NMC 811) with 95% active material content, a specific capacity of 175 mAh/g, a nominal

voltage of 3.7 V vs Li/Li⁺, and an area capacity of 3.5 mAh/cm² (± 0.1 mAh/cm²) was also purchased from Customcells Holding GmbH and was single-side coated on 20 μ m thick aluminum current collector foils.

2.2 Sample preparation

2.2.1 HE and bulk polymer film manufacturing

A series of HEs and bulk polymer (pBPAMA) films were prepared as follows. All samples were prepared inside a glovebox under a dry argon atmosphere (<1 ppm H₂O, <1 ppm O₂). In paper I and II the liquid electrolyte was prepared by mixing PC and EC with a 50:50 weight ratio, with the EC pre-heated to 60 °C. The lithium salt LiTFSI was then added to the solvent mixture to achieve a 1 M concentration. In paper III and IV an equivalent commercial electrolyte was utilized. For the preparation of HE films, the electrolyte was combined with the monomer BPAMA and the thermal initiator AIBN, with AIBN corresponding to 1 wt% of the monomer content. The liquid electrolyte content varied between 40, 45, and 50 wt% of the total weight. For the pBPAMA films, the monomer was mixed with 1 wt% AIBN and a small amount (around 10 wt%) of the solvent mixture (EC:PC 50:50 wt%) to dissolve the initiator. The chemicals were stirred until a homogeneous mixture was achieved. In paper III, CB was incorporated into the resins using two different mixing methods. In the first method, CB was mixed with the liquid electrolyte at varying contents of 0, 0.5, and 0.8 wt% of the total weight, followed by mixing with the monomer. In the second method, the CB content was increased to 1 and 1.5 wt% of the total weight, with CB first mixed with the monomer and then with the liquid electrolyte. The second approach enabled higher CB contents in the resins, which would have resulted in excessive viscosity using the first method. Comparative analysis showed that the microstructure and properties were consistent with both methods at these concentrations. Therefore, to avoid redundancy in the present work, the results were reported only once.

The HE and pBPAMA resins were then poured into aluminum molds (30 × 6 × 0.5 mm³) and covered with glass slabs. The specimens were clamped at both edges and vacuum-sealed in a pouch bag inside the glovebox. The bagged samples were then transferred out of the glovebox and thermally cured at 90 °C for 45 minutes in a preheated oven. Henceforth, the prepared HE samples are denoted as HE-45wt%-xxwt% where xx represents the CB content percentage (xx varying between 0-1.5).

2.2.2 HE-infused electrode and half-cell manufacturing

HE-impregnated LFP and NMC electrodes were prepared using a vacuum infusion process and assembled into half-cells in a pouch cell format. The cathodes were cut into strips approximately 15 mm × 100 mm and taped onto a 60 mm × 180 mm glass plate. The electrodes were then covered with a release film (perforated polyethylene) and breather fabric (coarse polyester felt cloth distribution medium). The entire setup was vacuum-sealed with rubber tapes and dried in a vacuum oven at 60 °C for 24 hours. The HE resin was prepared in a glovebox with a dry argon atmosphere (<1 ppm H₂O, <1 ppm O₂) by mixing the commercial electrolyte with the monomer BPAMA and AIBN, where AIBN was 1 wt% relative to the monomer weight, and the liquid electrolyte content varied between 45-50 wt% of the total weight. The mixture was sealed with a septum and used for vacuum infusion of the prepared setup with commercial electrodes outside the glovebox. Once the infusion was complete, the samples were thermally cured at 90 °C for 45 minutes. After curing, the cathode lamina was removed from the vacuum bag setup in the glovebox, cut into two approximately 15 mm × 30 mm infused electrodes, and each was placed into a pouch cell (70 mm × 70 mm) with an aluminum current collector. Lithium metal foil was used as the counter electrode with a nickel current collector, and a 250 μm Whatman glass-microfiber filter was used as a separator between electrodes. To ensure ionic conduction, about 300 μL of additional liquid electrolyte was added to wet the separator. Henceforth, the prepared HE-infused electrodes are denoted as HE-xxwt%-LFP and HE-xxwt%-NMC where xx represents the liquid electrolyte content percentage (45 or 50). For comparison, reference samples of non-infused LFP and NMC were assembled into pouch cells using the same setup with aluminum current collectors, lithium metal as the counter electrode with nickel current collectors, and the Whatman filter as the separator, with approximately 300 μL of liquid electrolyte added to wet the separator.

2.3 Characterization techniques

2.3.1 Microscopy characterization

Microscopy techniques were used to study the morphology and microstructure of the polymer skeleton of HEs (Paper I-III) and the comparison of them to pBPAMA (Paper I). Prior to analysis, both pBPAMA and HEs samples underwent a 24-hour leaching in deionized water on a shaking table to extract the liquid electrolyte (EC, PC, and LiTFSI) contained within the percolating polymer network. Subsequently, the samples were dried in a vacuum oven for

24–48 hours at 60 °C. The morphology of the HE-infused electrodes was also studied with microscopy techniques (Paper IV). In this case, the samples were not leached but instead were dried directly in a vacuum oven for 24–48 hours at 60 °C.

Scanning electron microscopy

Scanning electron microscopy (SEM) was used throughout this research to image the samples. Two SEM instruments were employed: a Hitachi SEM S-4800 equipped with a cold field-emission electron source and a Zeiss Gemini 450 (Paper II), and a Zeiss Ultra 55 FEG SEM equipped with a field emission electron gun (Paper III & IV). The pBPAMA (Paper II), HEs (Paper II & III) samples were submerged in liquid nitrogen and cryo-fractured in order to compare their morphology and microstructure. The fractured cross-sections were mounted on an SEM sample holder using conductive carbon tape and then coated (only for non-conductive samples) with a Pt/Pd layer using a Cressington 208HR sputter coater for 20 seconds, resulting in approximately 3 nm of conductive coating as measured by a quartz crystal microbalance, at a current of 80 mA. The coating layer was necessary to overcome the charging effect that affects non-conductive samples during SEM analysis, helping the dissipation of excess electrons and thus preventing the accumulation of electrical charge.

Broad ion beam

In Paper II–IV broad ion beam (BIB) was used to prepare SEM samples. A Leica EM TIC 3X triple ion-beam cutter was employed to produce finely polished, large cross-sectional surfaces for SEM analysis, thereby avoiding artifacts from manual manipulation, such as those caused by cryo-fracturing. Cross-sectioned samples of both HEs films and HE-infused electrodes, approximately 5 mm wide, were cut and adhered to a similarly sized Si wafer, which provides a perfectly flat surface for high-quality polishing. To minimize ion damage and thermal effects, the argon ion source was set at an energy level of 6–6.5 kV. All SEM images were captured at an accelerating voltage of 1 kV with a working distance of 3–9 mm.

Focused ion beam – scanning electron microscopy

Focused ion beam – scanning electron microscopy (FIB-SEM) was used to obtain a series of slicing images for reconstructing 3D models of the polymer with pores in the HEs (Paper I). These models were then used to analyze the pore size distribution and tortuosity. Additionally, the geodesic distance was

measured and compared to the Euclidean length. Furthermore, the reconstructed 3D models were utilized to develop finite element models of the HE.

FIB-SEM is a well-established technique for precise milling of samples, which offers higher precision, the capability for serial milling and imaging, better control over milling processes, enhanced resolution, versatility, and rapid sample preparation. FIB-SEM instruments consist of both an electron column and an ion column, arranged at an angle so that there is a fixed central position within the fields of view of both the SEM and FIB. For FIB-SEM sample preparation, a $\sim 2 \text{ mm}^3$ HE sample was glued to an aluminum stub using conductive silver paint. A 20 nm gold layer was then coated on the surface to enhance electrical conductivity. FIB-SEM milling and imaging were conducted using a Tescan GAIA3 (Tescan, Brno, Czech Republic) with a 30 keV Ga^+ ion beam. The beam current varied at different steps of the process. The specimen was initially tilted at 55° to the electron beam. A platinum layer approximately $2 \mu\text{m}$ thick was deposited on an area of $10 \times 20 \mu\text{m}^2$ using a 500 pA ion beam current. To obtain continuous slicing images of the sample, a T-shaped section was cut at the edge of the specimen using a 1 nA beam current. A reference pattern was milled onto the T-shape to serve as a location marker for subsequent cuts and imaging, helping to correct for any location errors caused by sample drift, as illustrated in Figure 3. The FIB milling and SEM imaging were controlled by a computer, starting at the end of the T-shape and gradually inward with a 20 nm step size using a low ion beam current of 269 pA. High-resolution images were captured in electron immersion mode with a pixel size of $10 \times 10 \text{ nm}^2$ and an electron beam spot size of 4 nm. The electron immersion mode generates an electromagnetic field that confines the electrons, leading to a stronger electron accumulation effect and resulting in sample drift, which significantly limits the number of images that can be captured. In this study, 80 images were acquired before the reference pattern drifted out of the reference window, with 60 images selected for 3D reconstruction. To minimize the charging effect, SEM images were obtained using the mid-angle backscattered electron detector, with the electron beam voltage set to 2 kV.

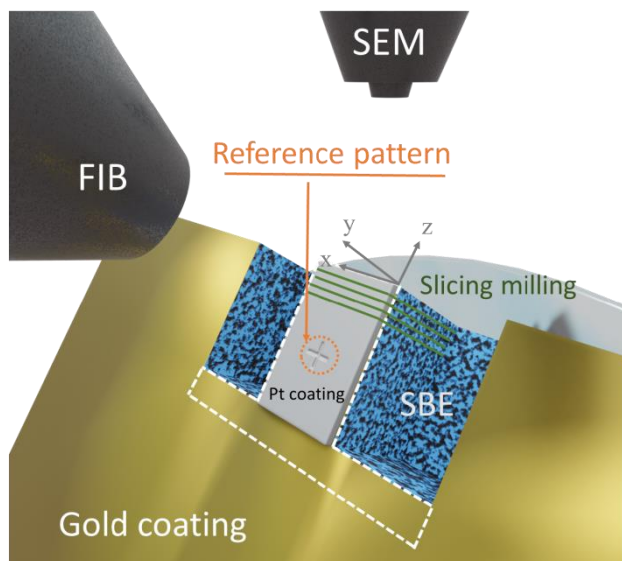


Figure 3: Illustration of the FIB-SEM setup. Adapted from reference [78].

2.3.2 Mechanical characterization

Dynamic mechanical analysis

Dynamic mechanical analysis (DMA) was performed to measure the experimental storage modulus of both the HEs and the bulk polymer films (Paper I). A TA Instruments DMA Q800 in tensile mode was used for this analysis. The specimen dimensions ranged from 4–5 mm in width, 0.4–0.55 mm in thickness, and 10–15 mm in length between the clamps. The thermal cycle for the measurement consisted of an initial isothermal step, where the temperature was held at 20 °C for 10 minutes to allow equilibration. This was followed by a temperature ramp at a heating rate of 3 °C min⁻¹ up to 200 °C. An amplitude of 8–13 μm was applied, which is less than 0.1% of the sample length.

2.3.3 Spectroscopy characterization

Fourier-transform infrared spectroscopy

The conversion of the PIPS reaction of HEs was evaluated via fourier-transform infrared spectroscopy (FTIR) in Papers I-III. A PerkinElmer Spectrum 100 instrument, equipped with a deuterated triglycine sulfate detector, was used to determine the double bond conversion of the methacrylate groups of the BPAMA monomer. The instrument featured a single reflection attenuated total

reflection (ATR) accessory unit with a diamond ATR crystal (Golden gate) from Graseby Specac Ltd. Data analysis was conducted using Spectrum software v. 10.5.1 from PerkinElmer. Two samples of each formulation were analyzed both before and after curing, with 16 scans performed for each spectrum at a resolution of 4 cm^{-1} . The conversion of the methacrylate groups was determined by comparing the area under the vinyl peak at 1637 cm^{-1} in uncured resin and cured films.

Nuclear magnetic resonance

Two different types of nuclear magnetic resonance (NMR) have been used in this thesis: the quantitative NMR for determination of the concentration of one or more chemical species in solution and diffusion NMR for determination of the diffusion coefficients of one or more chemical species in a solution. All sample preparation was performed inside a dry argon glovebox (as described in section 2.2.1) after which the samples were cut to approximately $10 \times 3 \times 0.5\text{ mm}^3$ to fit the NMR tubes. All the measurements were conducted at 298 K.

Quantitative NMR. Quantitative NMR was used to evaluate both the swelling and leaching of the pure polymer pBPAMA (Paper II) and the liquid electrolyte removal from HEs formulations (Papers II & III). When performing quantitative NMR, external references are needed to provide absolute concentrations because the acquired intensity has no unit. For the quantification of the amount of solvent and salt absorbed by pBPAMA (Paper II), the specimens were immersed in different electrolyte formulations to quantify the degree to which the electrolyte and/or solvent penetrates and swells the thermoset polymer.

The tests were conducted with the following formulations:

- 50:50 wt% EC without salt
- 1 M LiTFSI in 50:50 wt% EC:PC
- 2 M LiTFSI in 50:50 wt% EC:PC

The pBPAMA samples were then transferred into NMR tubes, and 600 μL of acetonitrile- d_3 was added before sealing them airtight. For the quantification of the liquid electrolyte removal from HEs, the samples were directly placed into NMR tubes after manufacturing and subsequently 600 μL of DMSO- d_6 (in Paper II) and 600 μL 1:1 w/w EC:PC (in Paper II & III) were added prior to sealing the tube airtight for ^1H and ^7Li quantification respectively. The amount of EC/PC released was monitored by ^1H NMR, using the peak integrals at 4.52 ppm for EC and at 4.85/4.02 ppm for PC. The amount of LiTFSI released was

tracked using ^{19}F and ^7Li NMR (with the Li : TFSI molar ratio maintained at 1:1 by electroneutrality). Quantitative data were obtained by relating the solvent (^1H) and salt (^7Li and ^{19}F) spectral integrals to those from external standard samples: ^1H (10 mg EC and 10 mg PC dissolved in 0.6 mL acetonitrile- d_3), ^7Li (TraceCERT®, 1000 mg L $^{-1}$ Li ions in dilute nitric acid), and ^{19}F (1 M LiTFSI in EC:PC 1:1). The uncertainty was estimated from the signal-to-noise ratio of the respective peaks in the sample [79].

Diffusion NMR. Diffusion NMR was used to determine the self-diffusion coefficients of the different electrolyte species (Paper II). Diffusion measurements were made using a GREAT60 gradient power supply that provides a maximum z-gradient strength of 1800 G/cm for the probe used. A stimulated echo pulse sequence was used with gradient duration δ set to between 0.8 – 1.0 ms, diffusion time Δ to 200 ms for ^{19}F , to 1000 ms for ^1H and to 800 ms for ^7Li measurements. The gradient strength g was stepped between 5 up to 500 and 1300 G/cm for different samples in 10 steps. The diffusional decay was fitted by Stejskal- Tanner (Equation 2.1) to obtain the diffusion coefficient D [80], where γ is the magnetogyric ratio and S and S_0 represent the integral intensities with and without gradient g , respectively.

$$S/S_0 = \exp(-\gamma^2 \delta^2 g^2 D [\Delta - \frac{\delta}{3}]) \quad (2.1)$$

The error of diffusion coefficient was estimated to be 4-5% by the uncertainty derived when fitting the Stejskal-Tanner expression using Levenberg-Marquardt fit.

2.3.4 Electrochemical characterization

Electrochemical Impedance Spectroscopy

Electrochemical impedance spectroscopy (EIS) was used to evaluate the conductivity of HEs both longitudinally-along the length of the films (Papers I-III) and transversely-across the thickness of the films (Paper III). The measurements were performed within a glovebox immediately after sample preparation to minimize the effects of solvent evaporation. Conductivity analysis of the HE films was conducted using a Gamry Series G 750 potentiostat/galvanostat/ZRA interface. For longitudinal conductivity measurements, a four-point electrode cell with gold wires was used, consisting of two working electrodes positioned 20 mm apart and two reference electrodes spaced 5 mm apart. For transverse conductivity measurements, HE discs (15 mm in diameter and 100 μm thick) were sandwiched between two stainless steel

blocking electrodes (15 mm in diameter) in a Swagelok-type cell. Impedance measurements were carried out over a frequency range of 120 kHz to 1 Hz. The bulk resistance (R_b) was determined by identifying the low-frequency intercept on the real axis of the resulting Nyquist plot. Conductivity (σ) was then calculated using Equation 2.2 where l represents the length between the reference electrodes (5 mm for the longitudinal conductivity, ca. 100 μm for the transversal conductivity), R_b is the bulk resistance, and A is the cross-sectional area of the sample (the rectangular cross section of the film for the longitudinal conductivity, the circular area of the disc for the transversal cross section).

$$\sigma = \frac{l}{R_b * A} \quad (2.2)$$

Cross-sectional area estimations were based on measurements of thickness, width and radius using a digital slide caliper. Three samples from each formulation underwent testing.

Galvanostatic cycling

In Paper IV, the HE-infused electrode half-cells were galvanostatically cycled between 2.6-3.9 V vs Li/ Li⁺ and 3.1-4.1 V vs Li/ Li⁺ for LFP and NMC respectively using a Neware CT-4008T-5V10mA-164 potentiostat at ambient temperature. For the first 10 cycles, in order to ensure a slow interphase formation for morphological studies, the applied current densities were 6.75 mA/g⁻¹ for LFP and 8.32 mA/g⁻¹ for NMC, corresponding to a C-rate of C/20. During a second stage, the LFP samples underwent longer term cycling for capacity retention test with applied current densities of 13.5 mA/g, 27 mA/g and 67.5 mA/g corresponding to a C-rate of C/10, C/5 and C/2 respectively. The capacities were calculated based on the areal capacity of the commercial electrodes. Reference samples of non-infused pristine LFP and NMC with 1M LiTFSI in EC:PC 1:1 v/v liquid electrolyte was also tested in the same way for comparison.

3 Results & Discussion

In this chapter, the key findings from this research on HEs are presented and analyzed. The results are organized by paper, addressing the primary research questions through a detailed examination of the structural, electrochemical, and mechanical properties of HEs. The first section presents the three-dimensional structural characterization of HEs, highlighting how pore architecture influences ionic conductivity and mechanical stability. The second section delves into the impact of varying porosity on ions mobility, providing insights into how morphological changes affect electrochemical performance. The third section examines the influence of nanosized CB in HEs formation and properties. Finally, the fourth section discusses the practical integration of HEs into commercial LIB electrodes, evaluating their performance during cycling and their potential for large-scale applications.

3.1 Paper I: 3D reconstruction and modelling of HE, theoretical models vs experimental data

The ionic conductivity of the HE is enabled by the liquid electrolyte within the porous polymer structure. Key factors such as the quantity, size, morphology, and particularly the interconnectivity of the pores significantly influence the ionic conductivity. Traditional 2D SEM micrographs are insufficient for characterizing the HE microstructure. For instance, pores in a 2D image often appear isolated, which does not align with the practical viability of the SBE. This discrepancy arises because pores that seem insulated in 2D may be interconnected in the 3D space through intricate zigzag pathways. Such connectivity, or tortuosity, cannot be determined from individual 2D images. Therefore, serial FIB/SEM imaging and subsequent 3D reconstruction emerges

as the most viable method for characterizing the HE. Moreover, the use of the FIB milling is advantageous because it eliminates the need for manual sample preparation (such as cryo-fracturing), which can introduce artifacts, ensuring more accurate and reliable morphology characterization. Previous studies have demonstrated the feasibility of characterizing pore structures using FIB-SEM [81-85].

In Paper I, the 3D structure of the HE with 45 wt% liquid content was reconstructed based on SEM imaging of consecutive FIB milled surfaces. The sample micrographs were subsequently analyzed using the finite element method (FEM). An illustration of the process is shown in Figure 4. Characterization of the 3D structure provided information on the diameter and volume distributions of pores in the polymer skeleton, as well as tortuosity. Numerical analyses provided predictions of elastic modulus and ionic conductivity of the bi-continuous HE material which were compared with the experimental values in order to evaluate the reliability of the model.

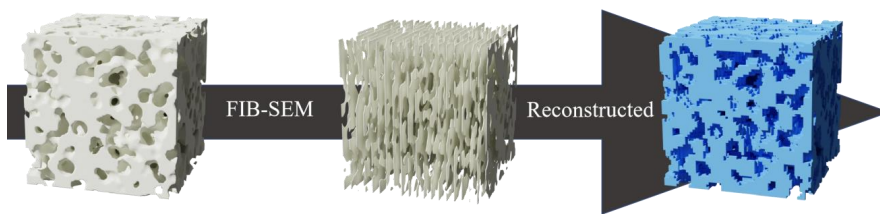


Figure 4: Illustration of 3D reconstruction of the HE. Adapted from reference [78].

3.1.1 3D reconstruction of the HE

Serial high-resolution images of the HE were obtained using FIB-SEM. This technique allows precise milling and high-resolution imaging at the nanometer scale. The images were processed to mitigate common artifacts such as the curtaining effect, which appears as vertical stripes due to varying milling rates in different phases of the porous structure (polymer and pores). A HE volume of approximately $5.4 \times 6.3 \times 1.2 \mu\text{m}^3$ was successfully reconstructed in 3D. The 3D model is presented in Figure 5. The polymer phase is marked in blue and the pore phase in orange. The pixel size in the micrographs is $10 \times 10 \text{ nm}^2$. The models are voxel-based where each pixel is converted into a voxel volume of $10 \times 12.2 \times 20 \text{ nm}^3$. The mean equivalent diameter was found to be 180 nm for the polymer segments and 160 nm for the pores, respectively.

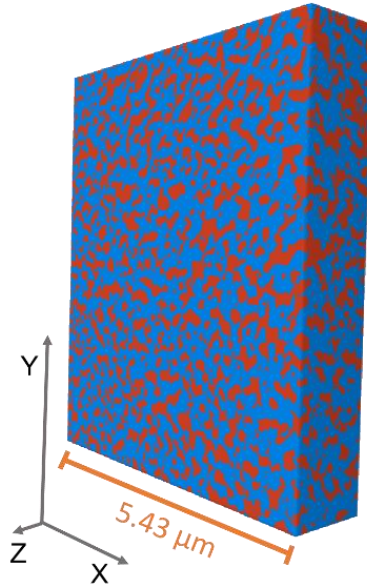


Figure 5: 3D reconstructed model of polymer phase (blue) and pore phase (orange). Adapted from reference [86].

A 6-connected analysis was performed in order to determine the presence of isolated pores in the HE microstructure. In the analysis, if any of the six faces of a voxel is shared with another voxel, the two voxels are identified as being connected. The results of the analysis determined that 99.3% of the pores were interconnected. This finding aligns with the results of a leaching test, which showed that the weight difference of the HE before and after removing the liquid electrolyte phase closely matched the weight of the liquid phase added during fabrication. This proves the formation of a bicontinuous percolating network.

3.1.2 Geodesic tortuosity

Geodesic tortuosity is defined as the ratio of the shortest path distance between two points (L) to the straight-line distance between them (L_0), also known as the Euclidean distance, as shown in Equation 3.1. An illustration of the definition is also given in Figure 7 (a).

$$\text{Geodesic tortuosity} = \frac{L}{L_0} \quad (3.1)$$

A higher geodesic tortuosity indicates a longer travel path for lithium ions, often resulting in reduced ionic conductivity. The 3D model of the HE pores was

converted into a skeleton dense graph, which consists of nodes and edges. The nodes represent the locations of the pores, and the edges represent the shortest paths between them. Compared to the 3D voxel mesh model, the skeleton graph is easier to analyze and compute. As illustrated in Figure 7 (b), the shortest paths between pores can be calculated using the skeleton graph. The skeleton dense graph has sufficiently high resolution to accurately analyze the pathways through the pores.

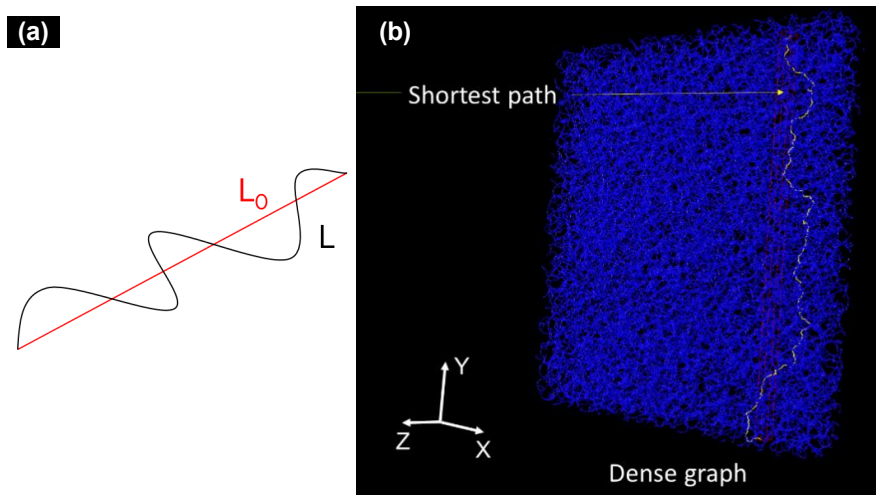


Figure 7: (a) Illustration of geodesic tortuosity. (b) The shortest paths computed from the skeleton dense graph. Adapted from reference [78].

By examining the shortest paths in the x, y, and z directions, the geodesic tortuosity in different directions was determined and the results are shown in Table 1. The geodesic tortuosity is consistent across all three directions confirming the isotropy of the HE. However, a slightly lower tortuosity is observed in the z direction due to the lower spatial resolution (20 nm), which tends to straighten highly tortuous paths. The average geodesic tortuosity, considering only the x and y directions, is 1.8. This indicates that lithium ions must travel 80% longer distances within the HE.

Table 1: Geodesic tortuosity of the HE in x, y, z directions. Adapted from reference [78].

	Geodesic tortuosity
x-direction	1.79
y-direction	1.81
z-direction	1.72

3.1.3 Simulated data vs experimental data

The topology data were utilized to numerically calculate both the elastic modulus and ionic conductivity. DMA and EIS analysis were performed to measure experimentally the storage modulus and the ionic conductivity, respectively. The simulated values were compared with the experimental ones as shown in Table 2.

Table 2: Experimental vs simulated values of storage modulus and ionic conductivity of HE. Adapted from reference [78].

	Experimental results	Simulation results
Storage modulus [MPa]	611	738
Ionic conductivity [mS/cm]	0.134	0.633

For the storage modulus, the simulated and experimental results are comparable, with the simulated modulus being slightly higher. This discrepancy is expected due to the stricter boundary conditions set in the FEM simulations. Regarding ionic conductivity, the simulation results overestimate the experimental values. This discrepancy can arise from several factors. Firstly, the resolution of the extracted image data ranges from 10 to 20 nm. As a result, pores smaller than 10 nm are not detected and thus are not included in the 3D model. Consequently, the numerical models likely consider pore structures that are too coarse for the given porosity, leading to an overestimation of ionic conductivity. Secondly, it is important to note that the FIB-SEM reconstructed model is based on a dry specimen, while the measured performance pertains to

a specimen in its wet state. In the wet state, the polymer is expected to absorb some of the liquid electrolyte and become swollen [87]. This swelling leads to lower porosity, reduced liquid content, and the potential closure of some narrow pathways. Additionally, the simulation model considers only normal diffusion according to Fick's law, whereas in reality, other effects such as migration, convection, and interaction with polymer walls may also play a role [88].

3.2 Paper II: effect of porosity on the ionic and molecular mobility in HEs

To better understand the effect of porosity on the ionic and molecular mobility, Paper II focuses on synthesizing a series of HEs via PIPS with liquid electrolyte content ranging from 40-50 wt%. The HE morphology depends on the reaction kinetics and mechanism as well as miscibility of the reagents, and composition of the reaction mixture [31, 32]. The conversion rate of the reactions was evaluated with FTIR. The ion conduction mechanism was investigated through a combination of morphological analysis and diffusion NMR studies. Diffusion NMR has often been utilized to study liquid dynamics in porous materials [89, 90]. Specifically, ^7Li and ^{19}F diffusion NMR has become one of the most precise methods for studying the mobility of charge carriers and lithium salt-polymer interactions in polymer electrolytes [91-95]. A distinct advantage of this technique is its ability to separately detect the movement of individual molecular and ionic components. Electrochemical performances were also evaluated with EIS.

3.2.1 Curing performance

FTIR was used to study the conversions for all the HEs formulations. Table 3 shows that a very high conversion of the double bond was achieved for all HEs with different liquid electrolyte content. The results show that thermal curing at the aforementioned conditions is a robust method for the PIPS in HEs systems.

Table 3: The average conversion of the different formulations calculated from FTIR peak intensities. Reprinted from reference [96].

Sample	Average conversion [%]
HE 40 wt%	95±1.0
HE 45 wt%	96±1.0
HE 50 wt%	95±2.0

3.2.2 Ionic and molecular mobility

To examine how electrolytes are distributed within HEs and their impact on ion conduction, we quantified the amounts of LiTFSI and EC/PC in HEs and pBPAMA through gravimetric analysis and NMR experiments. The gravimetric analysis on HEs showed that all the liquid electrolyte could be removed from the

samples, confirming the co-existence of two percolating phases. The release of LiTFSI, EC, and PC was monitored using quantitative NMR. In the HE samples with 45% liquid content, most of the LiTFSI was released within the first hour, and over 99 wt% was extracted within three hours. This rapid release indicates a continuous pore network that facilitates fast electrolyte transport. In contrast, the soaked pBPAMA films exhibited a much slower release, as the solvent molecule transport within the polymer network is significantly slower. The results for pBPAMA samples soaked in different electrolyte solutions upon saturation are summarized in Table 4. The findings show that both the solvent EC/PC and the lithium salt LiTFSI can be absorbed into the bulk polymer phase, with an uptake of approximately 8-10 wt% of the electrolyte. This “swelling” phenomenon occurs when a dry polymer is immersed in a solvent whose molecules can reversibly penetrate and expand the polymer network. The process eventually reaches equilibrium, as the elastic forces of the cross-links (either physical or chemical) counteract the volume expansion, impeding further solvent absorption [97]. Moreover, the individual compositions in Table 4 indicate that PC and EC were absorbed into pBPAMA at nearly a 1:1 weight ratio, and both solvents were absorbed more readily than LiTFSI. This is evidenced by the fact that the concentration of absorbed LiTFSI, relative to the absorbed solvent, is approximately 0.2-0.3 M, which is significantly lower than the original electrolyte's salt concentration of 1 M or 2 M.

Table 4: Solvents and salt release from soaked pBPAMA films. Adapted from reference [96].

Electrolytes concentration [M]	PC mass [mg]	EC mass [mg]	LiTFSI mass [mg]	Concentration of absorbed LiTFSI [M]
0	2.42	1.43	-	-
1	1.11	1.16	0.21	0.32
2	1.20	1.22	0.16	0.23

The ionic conductivity of the various HE formulations is summarized in Table 5. The liquid electrolyte exhibits conductivity one to two orders of magnitude higher than that of the HE samples. When the electrolyte content is reduced from 50 wt% to 40 wt%, the conductivity decreases sevenfold. This reduction in conductivity aligns with expectations, as the liquid phase within the HE is responsible for ion conduction, whereas the polymer phase does not contribute

to this process. However, it is surprising that increasing the electrolyte content from 40 wt% to 50 wt% results in a disproportionately large increase in conductivity compared to the increase in electrolyte-filled pore volume.

Table 5: Ionic conductivity results from EIS measurement. Adapted from reference [96].

Sample	Ionic conductivity [$10^{-4} \text{ S}\cdot\text{cm}^{-1}$]
1 M LiTFSI	43±4
HE 40 wt%	0.37±0.05
HE 45 wt%	1.4±0.1
HE 50 wt%	2.9±0.4

To understand the molecular mechanism behind this sharp increase, the diffusion of the cation (Li^+), anion (TFSI^-), and the solvents (PC and EC) within the HE was analyzed using NMR diffusion experiments. The self-diffusion coefficients, summarized in Figure 8, indicate that Li^+ , TFSI^- , and the carbonate molecules all diffuse more rapidly in HEs with higher electrolyte content, correlating well with conductivity values. Notably, Figure 8 (b) reveals that the reduction in solvent diffusion relative to its bulk value is significantly greater than that of Li^+ and TFSI^- diffusion.

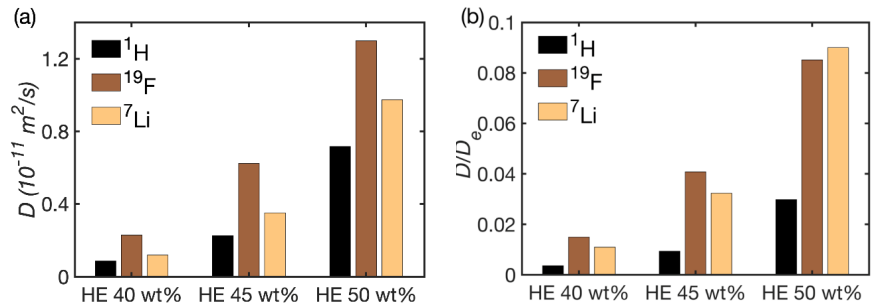


Figure 8: (a) The self-diffusion coefficients of ^1H (solvent), ^{19}F (anion) and ^7Li (cation) determined from HEs with 40 wt%, 45 wt% and 50 wt% liquid electrolyte content. (b) The ratio of ionic/molecular self-diffusion coefficients in HEs vs their respective bulk value in 1 M LiTFSI in EC/PC. Reprinted from reference [96].

3.2.3 Morphology and structure

Morphological analysis using SEM was performed on BIB prepared samples to better understand the dependence of conductivity and electrolyte species diffusion on the pore fraction and size. The micrographs of HE samples with 40 and 50 wt% liquid electrolyte content are shown in Figure 9. The milled surfaces of both specimens reveal the presence of macropores and mesopores, ranging from 200 nm down to less than 10 nm, and appear homogeneous at the micrometer scale, as seen in the lower magnification image in Figure 9 (a-b). The average pore diameter is 41 nm for the 40 wt% sample and 48 nm for the 50 wt% sample. This interconnected porous network, filled with electrolyte, serves as the ion transport pathway, contributing to the ion conductivity of the HEs. As the electrolyte content decreases, the presence of very narrow channels (<10 nm) is observed with increasing frequency. Within such narrow channels, the specific interactions between the electrolyte species and the channel walls greatly influence the self-diffusion coefficients [89, 98], as demonstrated for both solvents and ions in Figure 8 (a). In particular, based on the results shown in Table 4 and Figure 8 (b), the interactions between the channel walls and solvent molecules must be stronger than those between the walls and ions.

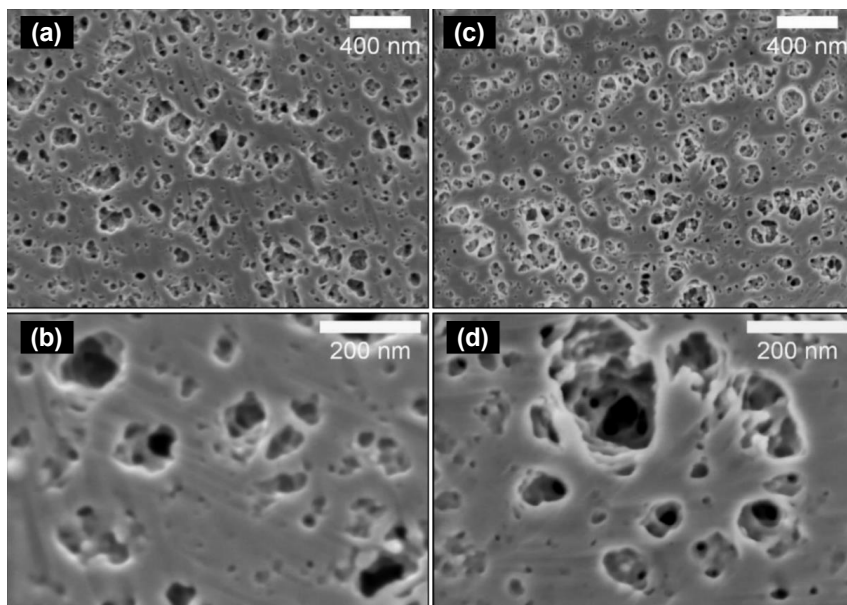


Figure 9: Cross-sectional SEM micrographs of **(a-b)** 40 wt% electrolyte content HEs **(c-d)** vs 50 wt% electrolyte content HEs at **(a-c)** lower magnifications and **(b-d)** higher magnifications. Reprinted from reference [96].

3.3 Paper III: effect of nanosized carbon black particles on HEs

This study investigates the influence of carbon black (CB) on the PIPS process for creating HEs suitable for LIB applications. A series of HEs with 45 wt% liquid content and with varying CB content ranging from 0-1.5 wt% was synthesized via PIPS. The research focuses on understanding how CB affects the PIPS process with particular focus on the resulting morphology and the ionic conductivity of the HEs. The conversion rate of the reactions was evaluated with FTIR. The ion conduction mechanism was investigated through a combination of morphological analysis and NMR studies. Density and volume differences were monitored through gravimetric analysis. Electrochemical performances were evaluated with EIS.

3.3.1 Curing performance

FTIR was used to determine the double bond conversion. The results are summarized in Table 6. The disappearance of the vinyl stretch peak at 1637 cm^{-1} indicated successful polymerization. The conversion rates were similar across all formulations, demonstrating high curing efficiency regardless of CB content. FTIR analysis confirmed that the addition of CB did not negatively impact the PIPS process. High conversion rates of double bonds were achieved in all HE samples, indicating that CB is compatible with the HE formation process.

Table 6: The average conversion of the different formulations calculated from FTIR peak intensities. Adapted from Paper III.

Sample	Average conversion [%]
HE-45wt%-0wt% CB	96±0.3
HE-45-wt%-0.5wt% CB	96±0.3
HE-45wt%-0.8wt% CB	96±0.2
HE-45wt%-1wt% CB	96±0.1
HE-45wt%-1.5wt% CB	96±0.3

3.3.2 Ionic and molecular mobility

To investigate the distribution of electrolytes within the different HE formulations and their correlation with conductivity, we measured the quantities of LiTFSI in the HEs using NMR experiments. The results are shown in Figure 10, where the relative LiTFSI on the y-axis is the mass of LiTFSI relative to the nominal LiTFSI content of the HE. As shown in Figure 10, for the sample without CB, all LiTFSI was released within the first hour, consistent with previous findings of Paper II. In CB-containing samples, the initial release amount was somewhat higher, and the release rate was slightly faster, except for the 1.5 wt% CB sample, which behaved similarly to the sample without CB. These results suggest a higher proportion of Li^+ distributed near the surface, potentially related to a skin layer structure, which will be discussed further in the following sections. The release process was completed within the first hour. Although the measured final release levels varied due to sample preparation differences (resulting in different initial lithium ion concentrations calculated as Li per HE masses), the similar kinetics indicate structural consistency across varying CB contents.

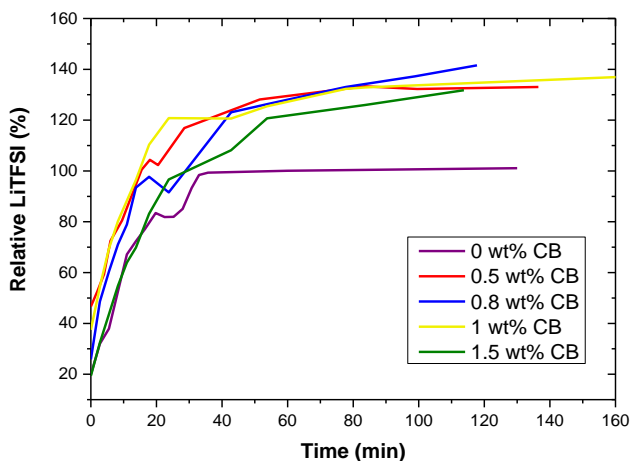


Figure 10: Amount of LiTFSI salt released from the HEs-45wt% with different CB content. Reprinted Paper III.

Density measurements of HEs with varying CB content show no significant differences, with densities around 1.2 mg/mm^3 before leaching and approximately 0.84 mg/mm^3 after leaching. The density decrease, about 30%,

and volumetric shrinkage, around 21%, are consistent across all formulations, aligning with literature [34]. These changes are attributed to the shrinkage of both the polymer matrix and the pores after liquid electrolyte removal and drying. Mass loss results indicate the complete extraction of the liquid electrolyte phase, confirming the presence of a percolating network and the coexistence of two phases as demonstrated in Papers I & II. The clear, colorless extracted electrolytes suggest that CB is primarily within the polymer phase. Conductivity measurements were taken both longitudinally and transversely, and the results are summarized in Table 7. The presence of CB enhanced the conductivity, with a noticeable increase observed with higher CB content. However, the transversal conductivity was significantly lower than longitudinal conductivity, likely due to the formation of a surface skin layer that hinders ionic transport across the sample thickness. This phenomenon is discussed further in the following section.

Table 7: Conductivity results from the EIS measurement. Adapted from Paper III.

Sample	Longitudinal Average Conductivity [10⁻⁴ S*cm⁻¹]	Transversal Average Conductivity [10⁻⁴ S*cm⁻¹]
HE-45wt%-0wt% CB	1.4±0.1	2.3±0.1
HE-45wt%-0.5wt% CB	2.3±0.2	0.4±0.3
HE-45wt%-0.8 wt% CB	3.3±0.6	0.2±0.1
HE-45wt%-1wt% CB	4.8±0.4	0.3±0.2
HE-45wt%-1.5 wt% CB	21±8	0.3±0.1

It has to be noted that the conductivity discussed in this section is both ionic and electronic due to the presence of CB which created an electron-conducting network. Since the pore morphology that primarily determines ionic conductivity remained constant (as discussed in the following section), the significant increase in conductivity was attributed to enhanced electronic conductivity through the percolating CB network. Although electronic conduction in battery electrolytes can lead to issues like electron leakage, energy

loss, or even short-circuiting, it can be beneficial within the electrode region, potentially improving ion conductivity as demonstrated in other systems [99].

3.3.3 Morphology and structure

SEM was used to analyze the morphology and microstructure of the polymer skeleton of the HEs. The micrographs of samples HE-45wt%-0.5wt% CB and HE-45wt%-1.5wt% CB (the two extreme CB contents investigated) are illustrated in Figure 11. SEM micrographs showed similar morphologies across all formulations, with macropores and mesopores ranging from 200 nm to less than 10 nm. SEM results indicated that CB did not significantly affect the overall morphology, confirming that the presence of CB did not alter the porous structure of the HEs.

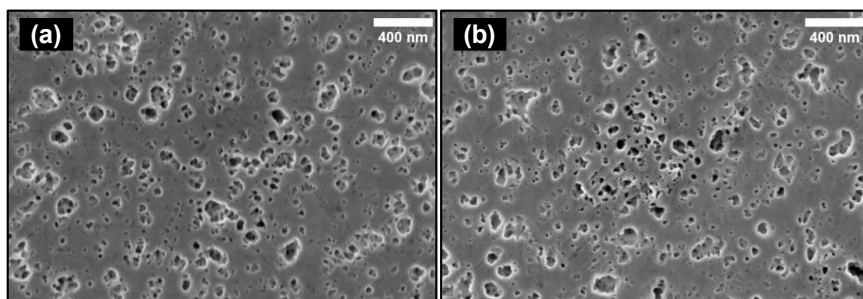


Figure 11: SEM micrographs of BIB polished cross-section of **(a)** HE-45wt%-0.5wt% CB and **(b)** HE-45wt%-1.5wt% CB. Reprinted from Paper III.

The presence of a surface skin layer was observed, particularly in samples with lower liquid electrolyte content as shown in Figure 12. However, varying the CB content did not influence the skin layer formation as the phenomenon was observed for samples with different CB content. The presence of the skin layer is likely responsible for the decrease in conductivity in the transversal direction shown in Table 7. To mitigate the formation of the surface skin layer, the liquid electrolyte phase content was increased to 50 wt% in a sample with 0.5 wt% CB. In certain regions of the sample, the skin layer was successfully removed, while in other regions, a much thinner skin layer was observed. Although the exact cause of the skin layer formation is still under investigation, one plausible explanation relates to the manufacturing process of the HE films [100]. The complex interplay between the interfacial tensions of the HE constituents and the processing conditions may create pressure gradients and flow. Related research has focused on suppressing the surface skin layer in freestanding monolithic membranes used in lithium-ion battery separators [76].

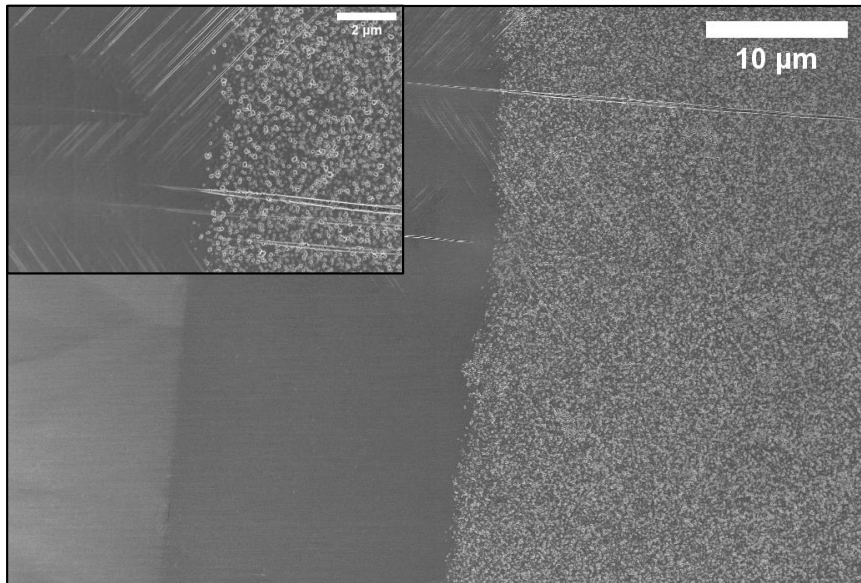


Figure 12: SEM micrographs of BIB polished cross-section of sample HE-45wt%-0.5wt% CB showing the surface skin layer at the edges of the specimen. The inset is at a higher magnification. Reprinted from Paper III.

3.4 Paper IV: HEs interactions with electrodes

This study explores the feasibility of using HEs synthesized via PIPS with commercial cathode, assessing their morphological and electrochemical stability after cycling. HE-infused electrodes were obtained by infusing the HE precursor with varying liquid content ranging from 45-50 wt% into commercial cathodes. Both nano-sized (LFP) and micron-sized (NMC) active material particles were infused and their morphology was analyzed before and after cycling. Additionally, the electrochemical performances of the infused electrodes half-cells at various C-rates were evaluated.

3.4.1 Infusion and PIPS in electrodes

BIB and SEM were used to investigate the morphology and microstructure of the HE-infused electrodes. A comparison between the non-infused pristine LFP electrode and HE-50wt%-LFP before cycling is shown in Figure 13. The results showed that the PIPS process effectively created a porous structure with micro- to mesopores, similar to previous studies on bulk HE samples. Both HE-50wt%-LFP and HE-45wt%-LFP exhibited non-uniform porosity, likely due to heterogeneities in the pristine active material particles, binders, and carbon black distributions.

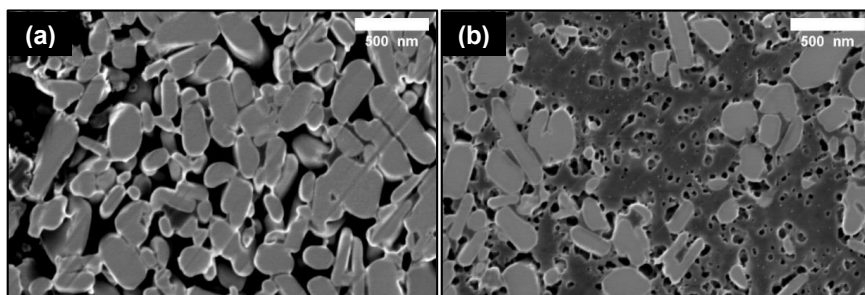


Figure 13: SEM micrographs of BIB polished cross-section of **(a)** pristine LFP electrode and **(b)** HE-50wt%-LFP electrode before cycling. Adapted from Paper IV.

The success of the PIPS process was also demonstrated in the case of micron-sized active material particles. A comparison between the non-infused pristine NMC electrode and HE-50wt%-NMC before cycling is shown in Figure 14. The NMC samples displayed a highly porous structure, effectively incorporating HEs between the micron-sized NMC particles.

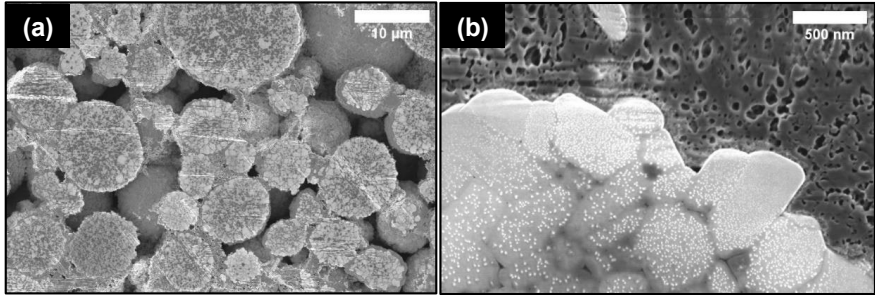
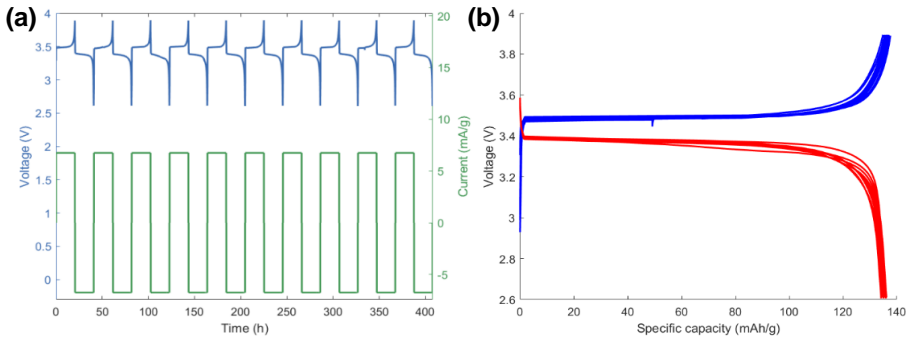


Figure 14: SEM micrographs of BIB polished cross-section of **(a)** pristine NMC electrode and **(b)** HE-50wt%-NMC electrode before cycling. Adapted from Paper IV.

3.4.2 Interface formation and stability

Galvanostatic cycling was performed on the HE-infused electrodes to assess their stability and electrochemical performance. 10 cycles at a low C-rate of C/20 were purposely chosen to let the electrode-electrolyte interface form slowly. The cycling data of the HE-50wt%-LFP electrode half-cell are shown in Figure 15.

Figure 15: Galvanostatic charge/discharge profiles of HE-50wt%-LFP



electrode half-cell with applied current density of 6.75 mA/g (C/20). **(a)** Voltage/current vs time plot. **(b)** Voltage vs specific capacity plot. Adapted from Paper IV.

The results of a reference sample containing only liquid electrolyte are shown in Figure 16 for comparison. The HE-50wt%-LFP electrode half-cell exhibited stable cycling behavior with a specific capacity around 135 mAh/g which is comparable with the specific capacity of the reference cell with liquid electrolyte, around 125 mAh/g. The similarity in specific capacity indicates that the HE can

effectively allow lithium-ion transport and maintain the electrochemical performance of the LFP electrode.

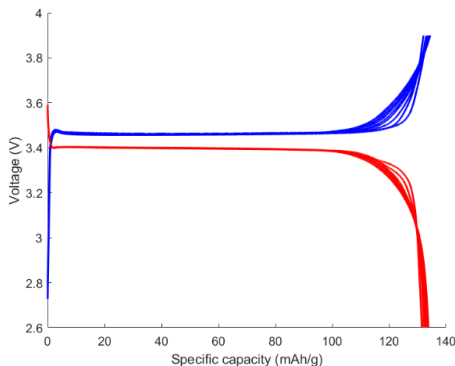


Figure 16: Galvanostatic charge/discharge profiles of the reference LFP electrode with liquid electrolyte half-cell with applied current density of 6.75 mA/g (C/20). Reprinted from Paper IV.

Similar results were obtained for the NMC samples. The fourth cycle of the HE-45wt%-NMC electrode half-cell and the reference one with only liquid electrolyte are shown in Figure 17, showing a comparable specific capacity of 124 mAh/g and 126 mAh/g respectively.

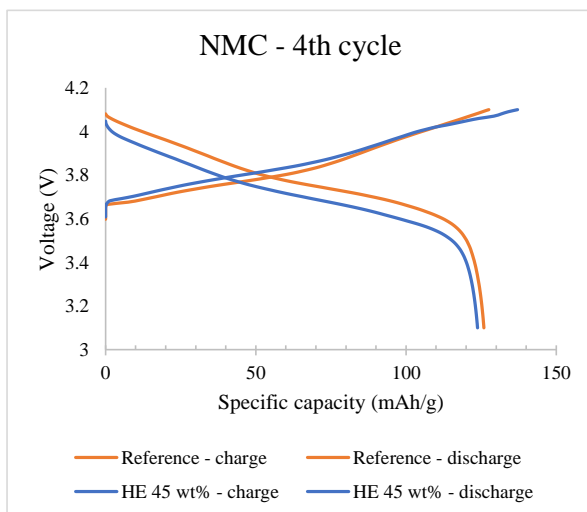


Figure 17: Galvanostatic charge/discharge profiles of the fourth cycle for HE-45wt%-NMC electrode and for the reference NMC electrode half-cells with applied current density of 8.32 mA/g (C/20). Reprinted from Paper IV.

The morphology of HE-50wt%-LFP after cycling (10 cycles at C/20) was analyzed with SEM as seen in Figure 18. Similar results were obtained for lower liquid electrolyte content. The micrographs after cycling revealed that the HE-infused electrodes maintained their morphological characteristics, indicating the resilience of the porous structure.

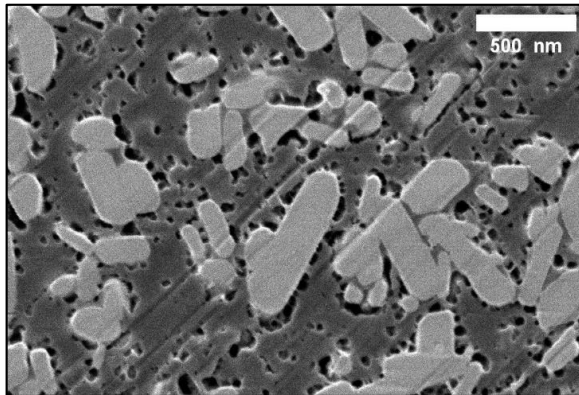


Figure 18: SEM micrographs of BIB polished cross-section of HE-50wt%-LFP electrode after cycling. Reprinted from Paper IV.

The successful infusion of HEs into the electrode particles and the subsequent stability of the infused electrodes during cycling were clearly demonstrated, not only between the particles, but also within the cracks present in the particles, as illustrated in Figure 19 for LFP and in Figure 20 for NMC. It is important to note that two types of cracks were observed in the samples: (1) cracks within the particles that contain infused HE, highlighting the effectiveness of the infusion, and (2) cracks between the active particles and the HE, which may indicate potential damage to the HE due to volume changes. However, the extent of these latter cracks is comparable to that seen in infused samples before cycling (Figure 13, Figure 20), suggesting that these cracks may have been introduced during the manufacturing process or SEM specimen preparation. This observation indicates that the HE-infused electrodes maintain their robustness under cycling conditions.

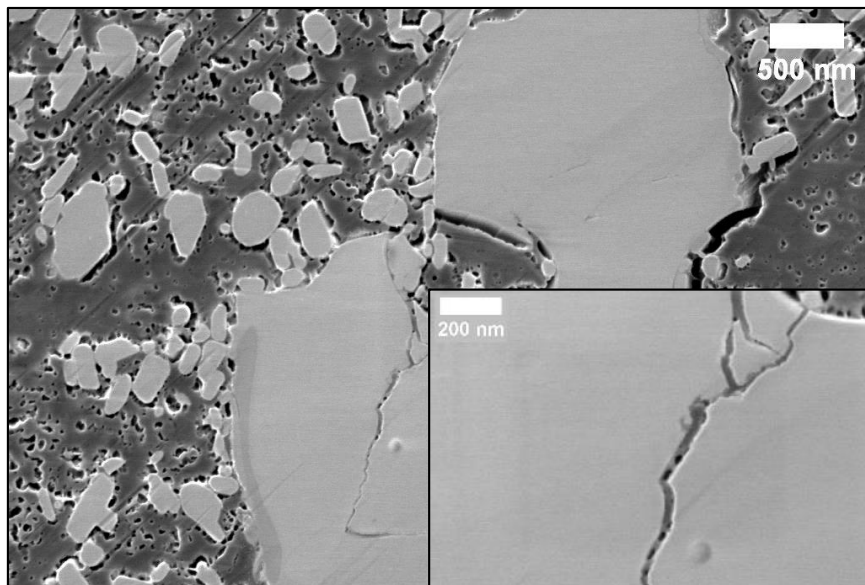


Figure 19: SEM micrographs of BIB polished cross-section of HE-45wt%-LFP electrode particle after cycling. The inset shows details of the porous phase-separated HE within LFP particle cracks. Reprinted from Paper IV.

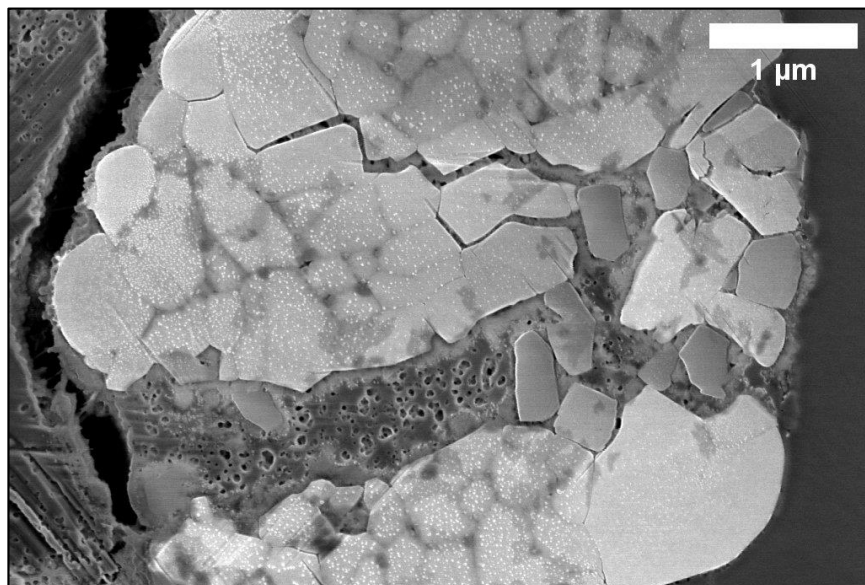


Figure 20: SEM micrographs of BIB polished cross-section of HE-50wt%-NMC electrode particle before cycling. Detail of the porous phase-separated HE within NMC particle cracks.

3.4.3 Cycling performance

The capacity retention test for the HE-50wt%-LFP electrode half-cell in Figure 21 showed stable specific capacity values across various cycling rates. The specific capacity shows a stable value equal to 120 mAh/g at C/10 which drops to 100 mAh/g at C/5. Instabilities are seen at C/2 with a further capacity drop. Finally, the specific capacity goes back to 120 mAh/g when a C-rate of C/10 is applied again. The cycling data demonstrates overall stability in the specific capacities across various cycling rates. Although a specific capacity drop was observed at higher C-rates, this behavior was expected due to increased internal resistance. Isolated instances where single data points deviate from the general trend are observed. These anomalies might be attributed to temporary inconsistencies. Importantly, subsequent cycles following these deviations return to the expected performance, indicating the resilience and recovery capability of the system. The cycling data demonstrated the overall stability and resilience of the HE-infused electrodes.

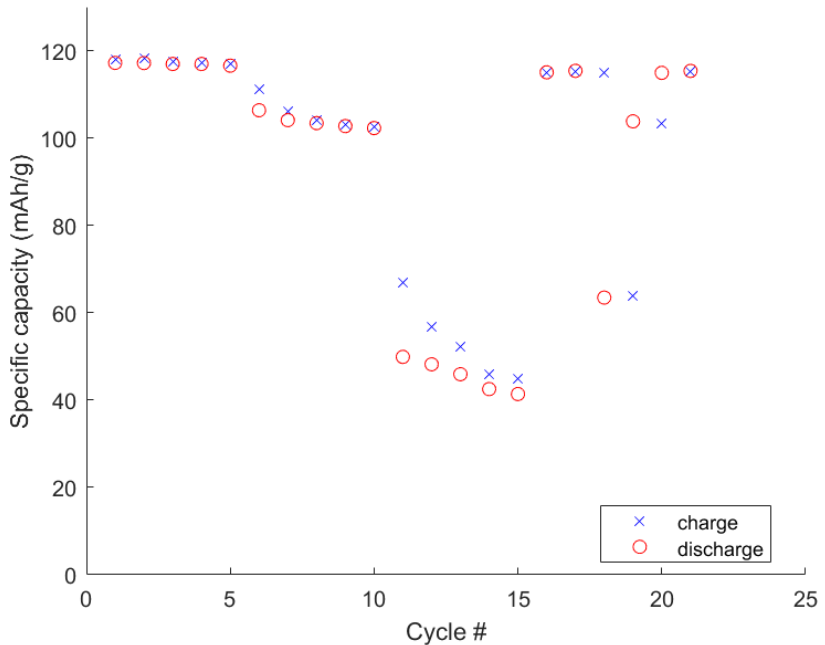


Figure 21: Capacity retention test of HE-50wt%-LFP electrode half-cell with applied current densities of 13.5 mA/g (C/10), 27 mA/g (C/5) and 67.5 mA/g (C/2).

4 Conclusions

This thesis has systematically advanced the development and understanding of HEs for LIBs, focusing on their structural, electrochemical, and multifunctional properties. Through the integration of experimental characterization, computational modeling, and practical application studies, this work developed a toolbox of characterization techniques for the study of HEs as key components in future generations of energy storage systems.

Paper I laid the groundwork by characterizing the structure of porous HEs in three dimensions using sequential FIB-SEM imaging. While the computational models successfully predicted the elastic modulus, the lithium-ion conductivity was overestimated, primarily due to the limitations in characterizing the wet state of the HEs. Nonetheless, this study establishes a robust experimental and computational methodology that can be applied to a variety of HE compositions, providing a foundation for future research in this area.

Building on this, Paper II explored the relationship between structure and performance of HEs through a combination of morphology study, conductivity measurement, and NMR analysis. The study demonstrates that both the solvent and lithium salt were absorbed into the bulk polymer phase, with a preferential absorption of solvent molecules. The results highlight the strong chemical interactions between the liquid and solid phases and the significant influence of narrow pores on ionic mobility. The results also show the importance of nano-scale morphology and of the interplay between the two different phases in determining the electrochemical performance of HEs.

Paper III focused on the influence of nanosized CB on HEs during the PIPS process, revealing that CB did not affect the chemical conversion or phase

separation but significantly enhanced the conductivity of HEs. This study confirmed the compatibility of CB with the PIPS process, resulting in consistent porous structures and fully percolating systems across all samples. The findings suggest that CB can be effectively utilized to optimize the electrochemical performance of HEs, supporting the development of more efficient and sustainable battery systems.

Finally, paper IV demonstrated the successful integration of HE within commercial electrode framework with both nanosized and micron-sized electrode active material particles. The infused electrodes maintained well-defined, phase-separated porous structures and exhibited stable electrochemical performance over multiple cycles. This study not only validated the compatibility of HEs with conventional cathodes but also highlighted the potential of PIPS in improving safety standards and streamlining the manufacturing process of LIBs by potentially eliminating the need for traditional PVDF binders.

In conclusion, this thesis has provided an improved comprehensive understanding of HEs' structural and functional properties and demonstrated their practical applicability in advanced battery systems.

5 Future Work

The findings presented in this thesis open several avenues for further research and development that could significantly enhance the performance, safety, and sustainability of HEs in LIBs.

One promising direction for future work is to explore HE infusion into a wider range of electrodes, including those with diverse active materials and morphologies. Investigating the compatibility of HEs with different cathodes and anodes could provide valuable insights into the versatility of HEs. Additionally, varying the liquid electrolyte content in these systems could further optimize the balance between mechanical strength and ionic conductivity, ultimately improving battery performance.

Long-term cycling stability studies are also critical areas that need further investigation. While this thesis demonstrated the initial compatibility and performance of HE-infused electrodes, extended cycling tests across various operating conditions—including temperature variations and higher current densities—will be essential to fully understand the durability and reliability of HEs in practical applications. Future research could explore the study of the voltage stability windows of HEs. Moreover, symmetrical cells, where both electrodes are identical, provide a simplified and controlled environment that allows for the direct observation of electrolyte behavior under various voltage conditions. Understanding the voltage stability of these electrolytes is crucial for optimizing their performance in practical battery systems, as it directly impacts their efficiency, safety, and longevity.

Advancing the characterization techniques used to study HEs could also yield deeper insights into their properties and behavior. While the research here

employed several powerful methods, future work could utilize more advanced and complementary techniques, such as X-ray photoelectron spectroscopy (XPS) to study chemical compositions and interfacial characteristics at the molecular level, or cryogenic electron microscopy (cryo-SEM and cryo-TEM) to provide high-resolution images of the electrolyte-electrode interfaces in their wet state. Additionally, atomic force microscopy (AFM) could be employed to investigate the surface topography and mechanical properties of HEs at the nanoscale, offering a more detailed understanding of their performance.

Building on the successful integration of HEs with conventional electrodes, another area of future research could focus on developing synthesis methods where HEs serve not only as electrolytes but also as binders. This approach would streamline the manufacturing process, reduce the number of components, and potentially eliminate the need for traditional binders like PVDF, contributing to more sustainable and cost-effective battery production. Exploring one-pot synthesis processes that incorporate HEs directly into the electrode slurry could innovate the way LIB electrodes are manufactured, leading to simpler, more efficient, and environmentally friendly production techniques.

Another promising area of investigation involves incorporating HEs as separators in lithium metal batteries. Lithium metal batteries are known for their high energy density, but they face significant safety concerns due to the formation of dendrites during lithium plating, which can lead to short circuits and thermal runaway [101]. HEs could serve as an effective solution by acting as a barrier that mitigates dendrite growth while maintaining ionic conductivity [102, 103]. Research in this direction could lead to safer, more reliable lithium metal batteries, potentially unlocking their use in high-performance applications where safety and energy density are paramount.

Given the significant carbon footprint of producing LIBs, with approximately 75 kg of CO₂ emissions generated for every 1 kWh of battery capacity produced [104], exploring alternative chemistries, such as monovalent elements like sodium [105] or potassium [106], or multivalent elements [107], presents another intriguing possibility for the application of HEs synthesized via PIPS. These alternative chemistries present advantages such as greater resource abundance and lower cost compared to lithium. Exploring HEs in these systems could reveal new insights into electrolyte behavior and stability across different chemical environments, potentially leading to the development of next-generation batteries with improved safety, cost-effectiveness, and

environmental sustainability. The adaptability of PIPS to various chemistries further underscores its potential as a versatile technique for enhancing battery performance in a wide range of energy storage technologies.

Another crucial direction for future research involves improving the sustainability of the HE components. This includes exploring bio-based or renewable sources for polymer matrices [108, 109] and electrolyte solvents [110], as well as investigating greener synthesis methods that reduce environmental impact. The development of biodegradable or recyclable components within HEs could significantly reduce the ecological footprint of lithium-ion batteries.

Finally, transitioning from laboratory-scale research to industrial-scale production is a crucial step toward the commercialization of HEs [111]. Future efforts should focus on scaling up synthesis and manufacturing processes, addressing challenges related to cost, reproducibility, and integration into existing production lines. Collaborations with industry partners could facilitate the development of scalable production methods and accelerate the adoption of HEs in commercial LIBs.

In summary, while this thesis has laid a solid foundation, the field of HE is ready ripe for further exploration. Continued research in these areas will not only refine our understanding but also contribute to the development of safer, more efficient, and sustainable energy storage technologies

6 Acknowledgments

I would like to acknowledge the Swedish Energy Agency (grant #48488) for funding the research presented in this thesis.

I would like to give special acknowledgment to my main supervisor, Professor **Mats Johansson**, for providing me with the opportunity to pursue my PhD studies and for his constant willingness to dedicate time to support and guide me throughout this journey. Thank you for always trusting me and giving me the freedom to develop both professionally and personally. I would also like to extend my gratitude to my co-supervisor, Professor **Fang Liu**, for her invaluable support of my research and personal growth as a scientist. Working with you has been one of the most inspiring and stimulating parts of my PhD. I would also like to acknowledge my other co-supervisor Professor **Göran Lindbergh** for his always precious and valuable scientific insights.

I would like to acknowledge my amazing colleagues in the Coating Division. Starting with my colleague and friend **Samuel** for always supporting each other from the very beginning. We started this together, we fought for this together and we are finishing this together. Surviving and partnering with you through this roller coaster was something I will never forget about: we made it, Sam! **Åsa**, not only for being a good colleague and an amazing friend, but also for making me feel at home in Sweden since the day we met. You and Scandi are two of the most incredible people I've ever met in my life. **Olivia**, for proofreading this thesis and for always being a dear friend of mine. I will never forget our Swedish and body pump classes, we nailed it! **Tijana**, (let's see if the spelling of your name is correct for once) for being the first one who made me feel comfortable in the Department. **Noemi**, for always being my best drinking

buddy. **Yanmiao**, for our yoga classes together and for your nice pep talks. My amazing office mate **Jorge**, for not being in the office but always ready with a joke when that was needed. **Natalia**, for being my Mediterranean buddy in Sweden. **Dan**, for always sharing valuable tips and advice and for being my favorite senior in the Division. **Arunika**, for being my best PhD-complaining buddy. And then also **Louise** and all the others for all the fun moments we shared together inside and outside KTH. I would like to extend my gratitude to the other seniors in the Division **Linda**, **Per-Olof** and **Eva** for always being there for useful tips and nice chats. **Alessio**, simply because this acknowledgment was meant to be. I can only wish you happiness and peacefulness for your future.

I would also like to acknowledge my colleagues in the Department of Chemical Engineering and in the Department of Aeronautical & Vehicle Engineering (only the good ones) for all the lab-related issues we solved together. The glovebox will remain my biggest nightmare in life. A special thanks to my friend **Elvira**, it was amazing to work with you. Dealing with a glovebox was a fair price to pay for having found a friend like you. And to **Alfredo**, for all the help you gave me with Matlab (I have lost count of the beers I owe you). Maybe I should also acknowledge the bad ones, because there is no better way to demonstrate what I am capable of than to be challenged in difficult situations.

I want to acknowledge some people outside KTH. A big acknowledgement goes to **Richard the Viking**, for making Sweden such a warmer place for me. Meeting you was definitely one of the best things that happened to me during this journey. I wish that more men were like you. **Danai**, you were there in the darkest moments of my Swedish adventure and you were my first true friend in Sweden. Our friendship is one of the biggest gains of this chapter of my life. **Cilla**, for always being an inspiration during my PhD. You are one of the most competent people I know and you are an amazing friend to have. **Acchia**, for being my sister with different blood. You are my favorite quadrangola in the entire world, we will always be each other's biggest fans. Ti quadro. **Kasra**, for the great support you gave me in the past 3 years. You have been an amazing life coach and our friendship helped me realize what I want in life. You will always have a special place in my heart. **Tio**, for being there for each other since day 1, always looking for our life direction together. Zio, ma che stiamo a fa oh? **Adri**, for always supporting each other throughout our life challenges and crazy ideas. We are seriously dangerous together! **Lorenzo**, **Tay** and **Bea**, for always being there to listen my complaints and help me forgetting about them with your great

company. **Kate**, for being my party girl buddy and my best Polish cook. **Elise**, for being my favorite bitchilante and Mediterranean partner in crime.

I would also like to acknowledge all my other friends in Italy, Spain, and around the world. If I named all of you I would need to write another PhD thesis. When you live in different cities and in different countries it's a challenge to find time to spend together but a true friendship doesn't fear distance and we are proving that. I love you all so much.

Last but not least, two people to whom my deepest acknowledgments go.

My sister **Petra**, for always being an example of excellence for me. You taught me so many life lessons, many more than what you are aware of. You taught me that in life nothing is for free and that you have to work hard to get your results. Your resilience and determination have always been truly inspiring for me. You are the smartest person I know. I love you.

Mia mamma **Gilda**, la prima persona a credere in me. Ci sei sempre stata per supportarmi e aiutarmi a trovare soluzioni. Senza di te questa tesi non esisterebbe (ma sul serio Ma). Tutto questo è per te, questo è il nostro PhD. Sei la donna più forte che io conosca. Grande Pilda, team gemelline sempre e per sempre. Ti voglio bene.

7 References

- [1] IPCC 2014, "Climate Change 2014: Synthesis Report. Contribution of Working Groups I, II, and III to the Fifth Assessment Report of the Intergovernmental Panel on Climate Change," *Geneva, Switzerland*, 2014.
- [2] IPCC 2021, "Climate Change 2021: The Physical Science Basis. Contribution of Working Group I to the Sixth Assessment Report of the Intergovernmental Panel on Climate Change," *Cambridge University Press*, 2021.
- [3] NASA Global Climate Change, "NASA Global Climate Change and Global Warming: Vital Signs of the Planet," 2008. [Online]. Available: <http://climate.nasa.gov/evidence> (accessed in July 2024)
- [4] The Paris Agreement, 2015. [Online]. Available: <https://unfccc.int/documents/9097> (accessed in July 2024)
- [5] H. Ritchie, "Sector by sector: where do global greenhouse gas emissions come from?," *Our World in Data*, 2020. [Online]. Available: <https://ourworldindata.org/ghg-emissions-by-sector> (accessed in July 2024)
- [6] United Nations. "The Sustainable Development Goals." <https://sdgs.un.org/goals> (accessed in July 2024).
- [7] M. Armand, P. Axmann, D. Bresser, M. Copley, K. Edström, C. Ekberg, D. Guyomard, B. Lestriez, P. Novák, M. Petranikova, W. Porcher, S. Trabesinger, M. Wohlfahrt-Mehrens, and H. Zhang, "Lithium-ion batteries – Current state of the art and anticipated developments," *Journal of Power Sources*, vol. 479, 2020, doi: 10.1016/j.jpowsour.2020.228708
- [8] M. Armand and J. M. Tarascon, "Building better batteries," *Nature*, vol. 451, no. 7179, pp. 652-657, 2008/02/01 2008, doi: 10.1038/451652a

- [9] A. Yoshino, "The Lithium-ion Battery: Two Breakthroughs in Development and Two Reasons for the Nobel Prize," *Bulletin of the Chemical Society of Japan*, vol. 95, no. 1, pp. 195-197, 2022, doi: 10.1246/bcsj.20210338
- [10] "The Nobel Prize in Chemistry 2019." <https://www.nobelprize.org/prizes/chemistry/2019/summary/> (accessed in July 2024).
- [11] M. Winter and R. J. Brodd, "What Are Batteries, Fuel Cells, and Supercapacitors?," *Chemical Reviews*, vol. 104, no. 10, pp. 4245-4270, 2004/10/01 2004, doi: 10.1021/cr020730k
- [12] R. A. Huggins, *Advanced Batteries: Materials Science Aspects*. 2008.
- [13] K. W. Beard, *Linden's Handbook of Batteries, Fifth Edition*. McGraw Hill LLC, 2019.
- [14] J. Kalhoff, G. G. Eshetu, D. Bresser, and S. Passerini, "Safer Electrolytes for Lithium-Ion Batteries: State of the Art and Perspectives," *ChemSusChem*, vol. 8, no. 13, pp. 2154-2175, 2015, doi: 10.1002/cssc.201500284
- [15] X. Huang, "Separator technologies for lithium-ion batteries," *Journal of Solid State Electrochemistry*, vol. 15, no. 4, pp. 649-662, 2010, doi: 10.1007/s10008-010-1264-9
- [16] P. Zhu, D. Gastol, J. Marshall, R. Sommerville, V. Goodship, and E. Kendrick, "A review of current collectors for lithium-ion batteries," *Journal of Power Sources*, vol. 485, 2021, doi: 10.1016/j.jpowsour.2020.229321
- [17] J. B. Goodenough and K.-S. Park, "The Li-Ion Rechargeable Battery: A Perspective," *Journal of the American Chemical Society*, vol. 135, no. 4, pp. 1167-1176, 2013/01/30 2013, doi: 10.1021/ja3091438
- [18] Y. Liu, R. Zhang, J. Wang, and Y. Wang, "Current and future lithium-ion battery manufacturing," *iScience*, vol. 24, no. 4, p. 102332, 2021/04/23/ 2021, doi: 10.1016/j.isci.2021.102332
- [19] Y. Chen, Y. Kang, Y. Zhao, L. Wang, J. Liu, Y. Li, Z. Liang, X. He, X. Li, N. Tavajohi, and B. Li, "A review of lithium-ion battery safety concerns: The issues, strategies, and testing standards," *Journal of Energy Chemistry*, vol. 59, pp. 83-99, 2021/08/01/ 2021, doi: 10.1016/j.jechem.2020.10.017
- [20] C. D. Rahn and C.-Y. Wang, *Battery Systems Engineering*. Wiley, 2013.
- [21] G. Pistoia, *Lithium-Ion Batteries: Advances and Applications*. Elsevier, 2014.
- [22] M. Pigłowska, Kurc, B., Galinski, M., Fuc, P., Kaminska, M., Szymlet, N., Daszkiewicz, P., "Challenges for Safe Electrolytes Applied in Lithium-Ion Cells-A Review," *Materials*, vol. 14, no. 22, p. 6783, 2021, doi: 10.3390/ma14226783

- [23] P. V. Wright, "Electrical conductivity in ionic complexes of poly(ethylene oxide)," *British Polymer Journal*, vol. 7, no. 5, pp. 319-327, 1975, doi: 10.1002/pi.4980070505
- [24] D. Zhou, D. Shanmukaraj, A. Tkacheva, M. Armand, and G. Wang, "Polymer Electrolytes for Lithium-Based Batteries: Advances and Prospects," *Chem*, vol. 5, no. 9, pp. 2326-2352, 2019, doi: 10.1016/j.chempr.2019.05.009
- [25] M. Armand, "Polymer solid electrolytes - an overview," *Solid State Ionics*, vol. 9-10, pp. 745-754, 1983/12/01/ 1983, doi: 10.1016/0167-2738(83)90083-8
- [26] M. Zhu, J. Wu, Y. Wang, M. Song, L. Long, S. H. Siyal, X. Yang, and G. Sui, "Recent advances in gel polymer electrolyte for high-performance lithium batteries," *Journal of Energy Chemistry*, vol. 37, pp. 126-142, 2019, doi: 10.1016/j.jechem.2018.12.013
- [27] X. Cheng, J. Pan, Y. Zhao, M. Liao, and H. Peng, "Gel Polymer Electrolytes for Electrochemical Energy Storage," *Advanced Energy Materials*, vol. 8, no. 7, p. 1702184, 2018, doi: 10.1002/aenm.201702184
- [28] A. Manuel Stephan, "Review on gel polymer electrolytes for lithium batteries," *European Polymer Journal*, vol. 42, no. 1, pp. 21-42, 2006/01/01/ 2006, doi: 10.1016/j.eurpolymj.2005.09.017
- [29] N. Ihrner, "Structural Lithium Ion Battery Electrolytes " Doctoral Thesis 2019.
- [30] N. Ihrner, W. Johannisson, F. Sieland, D. Zenkert, and M. Johansson, "Structural lithium ion battery electrolytes *via* reaction induced phase-separation," *Journal of Materials Chemistry A*, vol. 5, no. 48, pp. 25652-25659, 2017, doi: 10.1039/c7ta04684g
- [31] N. Shirshova, A. Bismarck, E. S. Greenhalgh, P. Johansson, G. Kalinka, M. J. Marczewski, M. S. P. Shaffer, and M. Wienrich, "Composition as a Means To Control Morphology and Properties of Epoxy Based Dual-Phase Structural Electrolytes," *The Journal of Physical Chemistry C*, vol. 118, no. 49, pp. 28377-28387, 2014, doi: 10.1021/jp507952b
- [32] N. Shirshova, T. Rogaume, H. Najmi, and M. Poisson, "The combustion behavior of epoxy-based multifunctional electrolytes," *Fire and Materials*, vol. 46, no. 1, pp. 192-204, 2021, doi: 10.1002/fam.2967
- [33] N. Shirshova, A. Bismarck, S. Carreyette, Q. P. V. Fontana, E. S. Greenhalgh, P. Jacobsson, P. Johansson, M. J. Marczewski, G. Kalinka, A. R. J. Kucernak, J. Scheers, M. S. P. Shaffer, J. H. G. Steinke, and M. Wienrich, "Structural supercapacitor electrolytes based on bicontinuous ionic liquid-epoxy resin systems," *Journal of Materials Chemistry A*, vol. 1, no. 48, 2013, doi: 10.1039/c3ta13163g
- [34] S. Emilsson, V. Vijayakumar, J. Mindemark, and M. Johansson, "Exploring the use of oligomeric carbonates as porogens and ion-

- conductors in phase-separated structural electrolytes for Lithium-ion batteries," *Electrochimica Acta*, vol. 449, 2023, doi: 10.1016/j.electacta.2023.142176
- [35] S. A. Chopade, J. G. Au, Z. Li, P. W. Schmidt, M. A. Hillmyer, and T. P. Lodge, "Robust Polymer Electrolyte Membranes with High Ambient-Temperature Lithium-Ion Conductivity via Polymerization-Induced Microphase Separation," *ACS Applied Materials & Interfaces*, vol. 9, no. 17, pp. 14561-14565, 2017/05/03 2017, doi: 10.1021/acsami.7b02514
- [36] S. A. Chopade, S. So, M. A. Hillmyer, and T. P. Lodge, "Anhydrous Proton Conducting Polymer Electrolyte Membranes via Polymerization-Induced Microphase Separation," *ACS Applied Materials & Interfaces*, vol. 8, no. 9, pp. 6200-6210, 2016/03/09 2016, doi: 10.1021/acsami.5b12366
- [37] L. D. McIntosh, M. W. Schulze, M. T. Irwin, M. A. Hillmyer, and T. P. Lodge, "Evolution of Morphology, Modulus, and Conductivity in Polymer Electrolytes Prepared via Polymerization-Induced Phase Separation," *Macromolecules*, vol. 48, no. 5, pp. 1418-1428, 2015, doi: 10.1021/ma502281k
- [38] M. W. Schulze, L. D. McIntosh, M. A. Hillmyer, and T. P. Lodge, "High-Modulus, High-Conductivity Nanostructured Polymer Electrolyte Membranes via Polymerization-Induced Phase Separation," *Nano Letters*, vol. 14, no. 1, pp. 122-126, 2014, doi: 10.1021/nl4034818
- [39] M. Chanda, *Introduction to Polymer Science and Chemistry: A Problem-Solving Approach*. CRC Press, 2013.
- [40] N. Nikfarjam, P. T. Coman, C. Free, P. Ziehl, M. Sadati, and R. E. White, "Advancing ionic conductivity in solid electrolytes: Insights from polymerization-induced phase separation and microstructural optimization," *Journal of Energy Storage*, vol. 93, p. 112287, 2024/07/15/ 2024, doi: 10.1016/j.est.2024.112287
- [41] J. P. Pender, G. Jha, D. H. Youn, J. M. Ziegler, I. Andoni, E. J. Choi, A. Heller, B. S. Dunn, P. S. Weiss, R. M. Penner, and C. B. Mullins, "Electrode Degradation in Lithium-Ion Batteries," *ACS Nano*, vol. 14, no. 2, pp. 1243-1295, 2020/02/25 2020, doi: 10.1021/acsnano.9b04365
- [42] S. Li, K. Wang, G. Zhang, S. Li, Y. Xu, X. Zhang, X. Zhang, S. Zheng, X. Sun, and Y. Ma, "Fast Charging Anode Materials for Lithium-Ion Batteries: Current Status and Perspectives," *Advanced Functional Materials*, vol. 32, no. 23, 2022, doi: 10.1002/adfm.202200796
- [43] E. Kamali-Heidari, A. Kamyabi-Gol, M. Heydarzadeh sohi, and A. Ataie, "Electrode Materials for Lithium Ion Batteries: A Review," *Journal of Ultrafine Grained and Nanostructured Materials*, vol. 51, no. 1, pp. 1-12, 2018, doi: 10.22059/jufgnsm.2018.01.01
- [44] W. Lee, S. Muhammad, C. Sergey, H. Lee, J. Yoon, Y. M. Kang, and W. S. Yoon, "Advances in the Cathode Materials for Lithium Rechargeable

- Batteries," *Angew Chem Int Ed Engl*, vol. 59, no. 7, pp. 2578-2605, Feb 10 2020, doi: 10.1002/anie.201902359
- [45] M. Thackeray, "Lithium-ion batteries: An unexpected conductor," (in eng), *Nat Mater*, vol. 1, no. 2, pp. 81-2, Oct 2002, doi: 10.1038/nmat736
- [46] S. Chen, X. Zhang, M. Xia, K. Wei, L. Zhang, X. Zhang, Y. Cui, and J. Shu, "Issues and challenges of layered lithium nickel cobalt manganese oxides for lithium-ion batteries," *Journal of Electroanalytical Chemistry*, vol. 895, p. 115412, 2021/08/15/ 2021, doi: 10.1016/j.jelechem.2021.115412
- [47] B. L. Ellis, K. T. Lee, and L. F. Nazar, "Positive Electrode Materials for Li-Ion and Li-Batteries," *Chemistry of Materials*, vol. 22, no. 3, pp. 691-714, 2010/02/09 2010, doi: 10.1021/cm902696j
- [48] W. B. Hawley and J. Li, "Electrode manufacturing for lithium-ion batteries—Analysis of current and next generation processing," *Journal of Energy Storage*, vol. 25, p. 100862, 2019/10/01/ 2019, doi: 10.1016/j.est.2019.100862
- [49] Q. Zhang, Z. Yu, P. Du, and C. Su, "Carbon nanomaterials used as conductive additives in lithium ion batteries," *Recent Pat Nanotechnol*, vol. 4, no. 2, pp. 100-10, Jun 2010, doi: 10.2174/187221010791208803
- [50] M.-J. Kleefoot, S. Enderle, J. Sandherr, M. Bolsinger, T. Maischik, N. Simon, J. Martan, S. Ruck, V. Knoblauch, and H. Riegel, "Enhancement of the wettability of graphite-based lithium-ion battery anodes by selective laser surface modification using low energy nanosecond pulses," *The International Journal of Advanced Manufacturing Technology*, vol. 118, no. 5, pp. 1987-1997, 2022/01/01 2022, doi: 10.1007/s00170-021-08004-3
- [51] C. M. Long, M. A. Nascarella, and P. A. Valberg, "Carbon black vs. black carbon and other airborne materials containing elemental carbon: Physical and chemical distinctions," *Environmental Pollution*, vol. 181, pp. 271-286, 2013/10/01/ 2013, doi: 10.1016/j.envpol.2013.06.009
- [52] X. Lu, G. J. Lian, J. Parker, R. Ge, M. K. Sadan, R. M. Smith, and D. Cumming, "Effect of carbon blacks on electrical conduction and conductive binder domain of next-generation lithium-ion batteries," *Journal of Power Sources*, vol. 592, p. 233916, 2024/02/01/ 2024, doi: 10.1016/j.jpowsour.2023.233916
- [53] Y. D. Yücel, E. Adolfsen, H. Dykhoff, J. Pettersson, S. Trey, M. Wysocki, E. Widenkvist Zetterström, D. Zenkert, R. Wreland Lindström, and G. Lindbergh, "Enhancing structural battery performance: Investigating the role of conductive carbon additives in LiFePO₄-Impregnated carbon fiber electrodes," *Composites Science and Technology*, vol. 251, p. 110571, 2024/05/26/ 2024, doi: 10.1016/j.compscitech.2024.110571
- [54] B. Chen, Z. Zhang, M. Xiao, S. Wang, S. Huang, D. Han, and Y. Meng, "Polymeric Binders Used in Lithium Ion Batteries: Actualities, Strategies

- and Trends," *ChemElectroChem*, vol. n/a, no. n/a, p. e202300651, 2024, doi: 10.1002/celec.202300651
- [55] ECHA - European Chemicals Agency. "Proposal to restrict PFAS." <https://echa.europa.eu/hot-topics/perfluoroalkyl-chemicals-pfas> (accessed in July 2024).
- [56] L. E. Asp, K. Bouton, D. Carlstedt, S. Duan, R. Harnden, W. Johannisson, M. Johansen, M. K. G. Johansson, G. Lindbergh, F. Liu, K. Peuvot, L. M. Schneider, J. Xu, and D. Zenkert, "A Structural Battery and its Multifunctional Performance," *Advanced Energy and Sustainability Research*, vol. 2, no. 3, p. 2000093, 2021, doi: 10.1002/aesr.202000093
- [57] L. E. Asp, M. Johansson, G. Lindbergh, J. Xu, and D. Zenkert, "Structural battery composites: a review," *Functional Composites and Structures*, vol. 1, no. 4, p. 042001, 2019, doi: 10.1088/2631-6331/ab5571
- [58] E. B. Gienger, P. A. T. Nguyen, W. Chin, K. D. Behler, J. F. Snyder, and E. D. Wetzel, "Microstructure and multifunctional properties of liquid + polymer bicomponent structural electrolytes: Epoxy gels and porous monoliths," *Journal of Applied Polymer Science*, vol. 132, no. 42, 2015, doi: 10.1002/app.42681
- [59] J. F. Snyder, E. D. Wetzel, and C. M. Watson, "Improving multifunctional behavior in structural electrolytes through copolymerization of structure- and conductivity-promoting monomers," *Polymer*, vol. 50, no. 20, pp. 4906-4916, 2009, doi: 10.1016/j.polymer.2009.07.050
- [60] D. J. O. B. James F. Snyder, Daniel M. Baechle, Daniel E. Mattson, and Eric D. Wetzel, "Structural Composite Capacitors, Supercapacitors, and Batteries for U.S. Army Applications," *ASME Conference on Smart Materials, Adaptive Structures and Intelligent Systems*, no. Ellicott City, Maryland, USA pp. 1-8, October 28-30 2008, doi: 10.1115/SMASIS2008-315
- [61] J. F. Snyder, R. H. Carter, and E. D. Wetzel, "Electrochemical and Mechanical Behavior in Mechanically Robust Solid Polymer Electrolytes for Use in Multifunctional Structural Batteries," *Chemistry of Materials*, vol. 19, no. 15, pp. 3793-3801, 2007, doi: 10.1021/cm070213o
- [62] W. Johannisson, N. Ihrner, D. Zenkert, M. Johansson, D. Carlstedt, L. E. Asp, and F. Sieland, "Multifunctional performance of a carbon fiber UD lamina electrode for structural batteries," *Composites Science and Technology*, vol. 168, pp. 81-87, 2018, doi: 10.1016/j.compscitech.2018.08.044
- [63] W. Johannisson, D. Zenkert, and G. Lindbergh, "Model of a structural battery and its potential for system level mass savings," *Multifunctional Materials*, vol. 2, no. 3, 2019, doi: 10.1088/2399-7532/ab3bdd
- [64] Y. D. Yücel, D. Zenkert, R. W. Lindström, and G. Lindbergh, "LiFePO₄-coated carbon fibers as positive electrodes in structural batteries:

- Insights from spray coating technique," *Electrochemistry Communications*, vol. 160, 2024, doi: 10.1016/j.elecom.2024.107670
- [65] Y. D. Yücel, E. Adolffson, H. Dykhoff, J. Pettersson, S. Trey, M. Wysocki, D. Zenkert, R. Wreland Lindström, and G. Lindbergh, "Powder-impregnated carbon fibers with lithium iron phosphate as positive electrodes in structural batteries," *Composites Science and Technology*, vol. 241, 2023, doi: 10.1016/j.compscitech.2023.110153
- [66] J. Xu, Z. Geng, M. Johansen, D. Carlstedt, S. Duan, T. Thiringer, F. Liu, and L. E. Asp, "A multicell structural battery composite laminate," *EcoMat*, vol. 4, no. 3, 2022, doi: 10.1002/eom2.12180
- [67] J. Xu, W. Johannisson, M. Johansen, F. Liu, D. Zenkert, G. Lindbergh, and L. E. Asp, "Characterization of the adhesive properties between structural battery electrolytes and carbon fibers," *Composites Science and Technology*, vol. 188, 2020, doi: 10.1016/j.compscitech.2019.107962
- [68] K. Bouton, L. Schneider, D. Zenkert, and G. Lindbergh, "A structural battery with carbon fibre electrodes balancing multifunctional performance," *Composites Science and Technology*, p. 110728, 2024/06/25/ 2024, doi: 10.1016/j.compscitech.2024.110728
- [69] R. Harnden, D. Carlstedt, D. Zenkert, and G. Lindbergh, "Multifunctional Carbon Fiber Composites: A Structural, Energy Harvesting, Strain-Sensing Material," *ACS Applied Materials & Interfaces*, vol. 14, no. 29, pp. 33871-33880, 2022, doi: 10.1021/acsami.2c08375
- [70] E. Jacques, Kjell, M., Zenkert, D., Lindbergh, G., Behm, M., "Impact of mechanical loading on the electrochemical behaviour of carbon fibers for use in energy storage composite materials.," *ICCM18 International Conferences on Composite Materials 18*, 2011.
- [71] M. H. Kjell, E. Jacques, D. Zenkert, M. r. Behm, and G. r. Lindbergh, "PAN-Based Carbon Fiber Negative Electrodes for Structural Lithium-Ion Batteries," *Journal of The Electrochemical Society*, vol. 158, no. 12, 2011, doi: 10.1149/2.053112jes
- [72] E. Jacques, M. H. Kjell, D. Zenkert, G. Lindbergh, M. Behm, and M. Willgert, "Impact of electrochemical cycling on the tensile properties of carbon fibres for structural lithium-ion composite batteries," *Composites Science and Technology*, vol. 72, no. 7, pp. 792-798, 2012, doi: 10.1016/j.compscitech.2012.02.006
- [73] E. Jacques, M. Hellqvist Kjell, D. Zenkert, G. Lindbergh, and M. Behm, "Expansion of carbon fibres induced by lithium intercalation for structural electrode applications," *Carbon*, vol. 59, pp. 246-254, 2013, doi: 10.1016/j.carbon.2013.03.015
- [74] E. Jacques, M. H. Kjell, D. Zenkert, and G. Lindbergh, "The effect of lithium-intercalation on the mechanical properties of carbon fibres," *Carbon*, vol. 68, pp. 725-733, 2014, doi: 10.1016/j.carbon.2013.11.056

- [75] Z. Zhang, D. Han, M. Xiao, S. Wang, Y. Feng, S. Huang, and Y. Meng, "New potential substitute of PVDF binder: poly(propylene carbonate) for solvent-free manufacturing high-loading cathodes of LiFePO₄|Li batteries," *Ionics*, vol. 29, no. 10, pp. 3895-3906, 2023/10/01 2023, doi: 10.1007/s11581-023-05108-6
- [76] K. Sakakibara, H. Kagata, N. Ishizuka, T. Sato, and Y. Tsujii, "Fabrication of surface skinless membranes of epoxy resin-based mesoporous monoliths toward advanced separators for lithium ion batteries," *Journal of Materials Chemistry A*, 10.1039/C6TA09005B vol. 5, no. 15, pp. 6866-6873, 2017, doi: 10.1039/C6TA09005B
- [77] A. J. Manly and W. E. Tenhaeff, "One-step fabrication of robust lithium ion battery separators by polymerization-induced phase separation," *Journal of Materials Chemistry A*, vol. 10, no. 19, pp. 10557-10568, 2022, doi: 10.1039/d1ta10730e
- [78] S. Duan, M. Cattaruzza, V. Tu, R. M. Auenhammer, R. Jänicke, M. K. G. Johansson, F. Liu, and L. E. Asp, "Three-dimensional reconstruction and computational analysis of a structural battery composite electrolyte," *Communications Materials*, vol. 4, no. 1, 2023, doi: 10.1038/s43246-023-00377-0
- [79] F. Malz and H. Jancke, "Validation of quantitative NMR," *Journal of Pharmaceutical and Biomedical Analysis*, vol. 38, no. 5, pp. 813-823, 2005, doi: 10.1016/j.jpba.2005.01.043
- [80] E. O. Stejskal and J. E. Tanner, "Spin Diffusion Measurements: Spin Echoes in the Presence of a Time-Dependent Field Gradient," *The Journal of Chemical Physics*, vol. 42, p. 288, 1965, doi: 10.1063/1.1695690
- [81] L. Holzer, F. Indutnyi, P. Gasser, B. Münch, and M. Wegmann, "Three-dimensional analysis of porous BaTiO₃ ceramics using FIB nanotomography," *Journal of Microscopy*, vol. 216, no. 1, pp. 84-95, 2004, doi: 10.1111/j.0022-2720.2004.01397.x
- [82] J. Joos, T. Carraro, A. Weber, and E. Ivers-Tiffée, "Reconstruction of porous electrodes by FIB/SEM for detailed microstructure modeling," *Journal of Power Sources*, vol. 196, no. 17, pp. 7302-7307, 2011/09/01/2011, doi: 10.1016/j.jpowsour.2010.10.006
- [83] N. Bassim, K. Scott, and L. A. Giannuzzi, "Recent advances in focused ion beam technology and applications," *MRS Bulletin*, vol. 39, no. 4, pp. 317-325, 2014/04/01 2014, doi: 10.1557/mrs.2014.52
- [84] C. Fager, S. Barman, M. Röding, A. Olsson, N. Lorén, C. von Corswant, D. Bolin, H. Rootzén, and E. Olsson, "3D high spatial resolution visualisation and quantification of interconnectivity in polymer films," *International Journal of Pharmaceutics*, vol. 587, p. 119622, 2020/09/25/ 2020, doi: 10.1016/j.ijpharm.2020.119622

- [85] C. Fager, M. Röding, A. Olsson, N. Lorén, C. von Corswant, A. Särkkä, and E. Olsson, "Optimization of FIB-SEM Tomography and Reconstruction for Soft, Porous, and Poorly Conducting Materials," (in eng), *Microsc Microanal*, vol. 26, no. 4, pp. 837-845, Aug 2020, doi: 10.1017/s1431927620001592
- [86] S. Duan, "Characterisation of a structural battery composite and its constituents," Department of Industrial and Materials Science, Chalmers University of Technology, Gothenburg, Sweden, 2022.
- [87] A. Sienkiewicz, P. Krasucka, B. Charnas, W. Stefaniak, and J. Goworek, "Swelling effects in cross-linked polymers by thermogravimetry," *Journal of Thermal Analysis and Calorimetry*, vol. 130, no. 1, pp. 85-93, 2017, doi: 10.1007/s10973-017-6131-9
- [88] B. Boz, T. Dev, A. Salvadori, and J. L. Schaefer, "Review—Electrolyte and Electrode Designs for Enhanced Ion Transport Properties to Enable High Performance Lithium Batteries," *Journal of The Electrochemical Society*, vol. 168, no. 9, 2021, doi: 10.1149/1945-7111/ac1cc3
- [89] F. Elwinger, P. Pourmand, and I. Furó, "Diffusive Transport in Pores. Tortuosity and Molecular Interaction with the Pore Wall," *The Journal of Physical Chemistry C*, vol. 121, no. 25, pp. 13757-13764, 2017, doi: 10.1021/acs.jpcc.7b03885
- [90] R. Valiullin, *Diffusion NMR of Confined Systems: Fluid Transport in Porous Solids and Heterogeneous Materials*. Cambridge: The Royal Society of Chemistry, 2017.
- [91] J. D. Jeon and S. Y. Kwak, "Variable-Temperature ^7Li Solid-State NMR Investigation of Li-Ion Mobility and Its Correlation with Conductivity in Pore-Filling Polymer Electrolytes for Secondary Batteries," *Macromolecules*, vol. 39, no. 23, pp. 8027-8034, 2006, doi: 10.1021/ma061521v
- [92] W. Gorecki, M. Jeannin, E. Belorizky, C. Roux, and M. Armand, "Physical properties of solid polymer electrolyte PEO(LiTFSI) complexes," *Journal of Physics: Condensed Matter*, vol. 7, no. 34, p. 6823, 1995, doi: 10.1088/0953-8984/7/34/007
- [93] K. Hayamizu, E. Akiba, T. Bando, and Y. Aihara, " ^1H , ^7Li , and ^{19}F nuclear magnetic resonance and ionic conductivity studies for liquid electrolytes composed of glymes and polyethenoglycol dimethyl ethers of $\text{CH}_3\text{O}(\text{CH}_2\text{CH}_2\text{O})_n\text{CH}_3$ ($n=3-50$) doped with $\text{LiN}(\text{SO}_2\text{CF}_3)_2$," *The Journal of Chemical Physics*, vol. 117, no. 12, pp. 5929-5939, 2002, doi: 10.1063/1.1501279
- [94] K. Timachova, H. Watanabe, and N. P. Balsara, "Effect of Molecular Weight and Salt Concentration on Ion Transport and the Transference Number in Polymer Electrolytes," *Macromolecules*, vol. 48, no. 21, pp. 7882-7888, 2015, doi: 10.1021/acs.macromol.5b01724

- [95] B. Sun, J. Mindemark, E. V. Morozov, L. T. Costa, M. Bergman, P. Johansson, Y. Fang, I. Furó, and D. Brandell, "Ion transport in polycarbonate based solid polymer electrolytes: experimental and computational investigations," *Physical Chemistry Chemical Physics*, vol. 18, no. 14, pp. 9504-9513, 2016, doi: 10.1039/C6CP00757K
- [96] M. Cattaruzza, Y. Fang, I. Furó, G. Lindbergh, F. Liu, and M. Johansson, "Hybrid polymer-liquid lithium ion electrolytes: effect of porosity on the ionic and molecular mobility," *Journal of Materials Chemistry A*, vol. 11, no. 13, pp. 7006-7015, 2023, doi: 10.1039/D3TA00250K
- [97] A. Gugliuzza, "Solvent Swollen Polymer," in *Encyclopedia of Membranes*, E. Drioli and L. Giorno Eds.: Springer Berlin Heidelberg, 2016, pp. 1801-1802.
- [98] D. C. Martínez Casillas, M. P. Longinotti, M. M. Bruno, F. Vaca Chávez, R. H. Acosta, and H. R. Corti, "Diffusion of Water and Electrolytes in Mesoporous Silica with a Wide Range of Pore Sizes," *The Journal of Physical Chemistry C*, vol. 122, no. 6, pp. 3638-3647, 2018, doi: 10.1021/acs.jpcc.7b11555
- [99] X. Guo, Z. Ju, X. Qian, Y. Liu, X. Xu, and G. Yu, "A Stable Solid Polymer Electrolyte for Lithium Metal Battery with Electronically Conductive Fillers," *Angew Chem Int Ed Engl*, vol. 62, no. 7, p. e202217538, Feb 6 2023, doi: 10.1002/anie.202217538
- [100] S. Dubinsky, J. I. Park, I. Gourevich, C. Chan, M. Deetz, and E. Kumacheva, "Toward Controlling the Surface Morphology of Macroporous Copolymer Particles," *Macromolecules*, vol. 42, no. 6, pp. 1990-1994, 2009/03/24 2009, doi: 10.1021/ma802813v
- [101] G. Yasin, M. Arif, T. Mehtab, X. Lu, D. Yu, N. Muhammad, M. T. Nazir, and H. Song, "Understanding and suppression strategies toward stable Li metal anode for safe lithium batteries," *Energy Storage Materials*, vol. 25, pp. 644-678, 2020/03/01/ 2020, doi: 10.1016/j.ensm.2019.09.020
- [102] P. Lennartz, B. A. Paren, A. Herzog-Arbeitman, X. C. Chen, J. A. Johnson, M. Winter, Y. Shao-Horn, and G. Bruncklaus, "Practical considerations for enabling Li|polymer electrolyte batteries," *Joule*, vol. 7, no. 7, pp. 1471-1495, 2023/07/19/ 2023, doi: 10.1016/j.joule.2023.06.006
- [103] Y. Pan, S. Chou, H. K. Liu, and S. X. Dou, "Functional membrane separators for next-generation high-energy rechargeable batteries," *National Science Review*, vol. 4, no. 6, pp. 917-933, 2017, doi: 10.1093/nsr/nwx037.8/22/2024
- [104] M. Song, H. Tan, D. Chao, and H. J. Fan, "Recent Advances in Zn-Ion Batteries," *Advanced Functional Materials*, vol. 28, no. 41, p. 1802564, 2018, doi: 10.1002/adfm.201802564
- [105] F. Gebert, J. Knott, R. Gorkin, S.-L. Chou, and S.-X. Dou, "Polymer electrolytes for sodium-ion batteries," *Energy Storage Materials*, vol. 36, pp. 10-30, 2021, doi: 10.1016/j.ensm.2020.11.030

- [106] X. Zhu, R. N. Ali, M. Song, Y. Tang, and Z. Fan, "Recent Advances in Polymers for Potassium Ion Batteries," *Polymers*, vol. 14, no. 24, p. 5538, 2022, doi: 10.3390/polym14245538
- [107] D. Kumar, L. R. Franco, N. Abdou, R. Shu, A. Martinelli, C. M. Araujo, J. Gladisch, V. Gueskine, R. Crispin, and Z. Khan, "Water-in-Polymer Salt Electrolyte for Long-Life Rechargeable Aqueous Zinc-Lignin Battery," *Energy & Environmental Materials*, p. e12752, doi: 10.1002/eem2.12752
- [108] C. Gioia, G. Lo Re, M. Lawoko, and L. Berglund, "Tunable Thermosetting Epoxies Based on Fractionated and Well-Characterized Lignins," *Journal of the American Chemical Society*, vol. 140, no. 11, pp. 4054-4061, 2018/03/21 2018, doi: 10.1021/jacs.7b13620
- [109] A. M. Nelson and T. E. Long, "A perspective on emerging polymer technologies for bisphenol-A replacement," *Polymer International*, vol. 61, no. 10, pp. 1485-1491, 2012, doi: 10.1002/pi.4323
- [110] A. von Wald Cresce and K. Xu, "Aqueous lithium-ion batteries," *Carbon Energy*, vol. 3, no. 5, pp. 721-751, 2021, doi: 10.1002/cey2.106
- [111] J. T. Frith, M. J. Lacey, and U. Ulissi, "A non-academic perspective on the future of lithium-based batteries," *Nature Communications*, vol. 14, no. 1, p. 420, 2023/01/26 2023, doi: 10.1038/s41467-023-35933-2

